Coordination Chemistry Reviews 253 (2009) 2935–2958

Contents lists available at ScienceDirect

Coordination Chemistry Reviews

journal homepage: www.elsevier.com/locate/ccr

Review

Theoretical calculations of structures and properties of one-dimensional silicon-based nanomaterials: Particularities and peculiarities of silicon and silicon-containing nanowires and nanotubes

Boon K. Teo [a,*], Shu-Ping Huang [b], R.Q. Zhang [b], Wai-Kee Li [c]

[a] Department of Chemistry, University of Illinois at Chicago, Chicago, IL 60607, USA
[b] Center of Super-Diamond and Advanced Films (COSDAF) & Department of Physics and Materials Sciences, City University of Hong Kong, Hong Kong SAR, China
[c] Department of Chemistry, The Chinese University of Hong Kong, Shatin, N.T., Hong Kong SAR, China

Contents

1. Introduction 2936
2. Atomic properties and bonding capabilities of silicon vs. carbon 2936
3. Silicon nanowires (SiNWs): tuning of electronic structures and manipulations of properties 2937
4. Silicon nanotubes (SiNTs): the Knowns and the Yet Unknowns 2939
   4.1. The sp^2 SiNTs 2940
      4.1.1. Single-walled sp^2 SiNTs 2940
      4.1.2. Double-walled sp^2 SiNTs 2943
      4.1.3. Predictions of the structures and properties of sp^2 SiNTs 2943
   4.2. The sp^3 SiNTs 2943
      4.2.1. Single-walled sp^3 SiNTs 2943
      4.2.2. Double-walled sp^3 SiNTs 2945
   4.3. Crystalline silicon nanotubes (cSiNTs) 2945
      4.3.1. Preparation of cSiNTs via various templates 2945
      4.3.2. Theoretical investigations of crystalline silicon nanotubes 2947
5. SiC nanowires (SiCNWs) 2947
6. Silicon carbide nanotubes (SiCNTs) 2949
   6.1. Synthesis of SiCNWs, biaxial SiC|SiO_2 NWs, and SiCNTs using CNTs as reactive templates 2949
   6.2. Theoretical studies of SiCNT structures 2950
      6.2.1. Single-walled sp^2 SiCNTs 2950
      6.2.2. Bundled sp^2 SiCNTs 2954
7. Nanotube–nanowire transformations 2954
   7.1. From SiNW ⊂ AuNT to AuNW ⊂ SiO_2NT: SiNWs as sacrificial templates 2954
8. Photoluminescence and band-gap opening in quantum-size regime 2954
   8.1. Photoluminescence 2954
   8.2. Band-gap opening and indirect-to-direct band-gap transformation 2955
9. Acronyms 2955
   9.1. Acronyms of various calculation methods, their applications and limitations 2956
   9.2. Other acronyms 2957
10. Conclusions 2957
   References 2958

ARTICLE INFO

Article history:
Received 12 July 2009
Accepted 3 August 2009
Available online 7 August 2009

ABSTRACT

Among various nanomaterials, one-dimensional silicon-based nanomaterials occupy a very important place because of their unique mechanical, thermal, optical, electrical, and optoelectronic properties, and potential technological applications. Herein, we review the recent theoretical calculations of the

* Corresponding author.
E-mail address: boonkteo@uic.edu (B.K. Teo).

0010-8545/$ – see front matter © 2009 Published by Elsevier B.V.
doi:10.1016/j.ccr.2009.08.001

Keywords:
Theoretical calculations
Structures and properties
Silicon-based nanomaterials
Silicon carbide nanostructures
Silicon nanowires and nanotubes

structures and properties of silicon-based nanowires and nanotubes, with special emphasis on the particularities and peculiarities of silicon and silicon-containing nanowires and nanotubes. These calculations allow not only rationalization of the observed experimental results, but also predictions of the yet-unknown nanostructures and their unusual properties.

1. Introduction

Nanomaterials are the bricks and mortars of nanoscience and nanotechnology. In the last two decades, a great effort has been devoted to nanomaterials research because physical properties of the nanostructured material such as the band-gaps and optical transitions can be continuously modified by controlling their size or shape (the so-called quantum-size effect). In fact, nanochemistry allows unprecedented changes of the fundamental properties of matters (often drastically different from those of the bulk phase), giving rise to novel materials and, ultimately, new applications.

Low-dimensional nanomaterials are of particular interest in that they may exhibit anisotropic and/or dimension-tunable properties, both of which are important attributes in nanodevice applications. Recently, two classes of one-dimensional (1D) nanomaterials, carbon nanotubes (CNTs) and silicon nanowires (SiNWs), have attracted much attention because of their unique properties. CNTs [1–5] possess highly interesting properties, such as small-diameter, high aspect ratio, high mechanical strength, high thermal and chemical stabilities, excellent heat conduction, unusual electrical and electronic properties, etc. [6–16] In fact, CNTs can be either metallic or semiconducting, with the semiconducting band-gap depending upon the tube diameter, geometry, and chirality. Since its discovery in 1991, CNTs have found its way into many industries.

Although silicon and carbon are from the same group (Group IV) in the Periodic Table, the two elements are very different in terms of their structural, chemical and physical properties. For example, while CNTs are relatively easy to make, the corresponding silicon nanotubes (SiNTs), composed of rolled-up graphite-like sheets, are difficult to synthesize.

1D SiNWs [17,18] are particularly important in nanotechnology because Si-based nanoelectronics is compatible with Si-based microelectronics. SiNWs in the nanosize regime have been shown to exhibit quantum confinement effects (e.g., band-gap opening and indirect-to-direct band-gap transformation upon size reduction) and they are expected to play a key role as interconnection and functional components in future nanosized electronic and optical devices.

Even more interesting are the hybrid nanomaterials comprising both silicon and carbon. They have certain advantageous attributes over pure carbon or pure silicon nanomaterials. For example, silicon carbide nanotubes (SiCNTs) are expected to have advantages over CNTs because they possess high reactivity on the exterior surface, facilitating sidewall decoration, and greater stability at high temperature [19]. And SiCNTs are theoretically predicted to be better materials for hydrogen storage than pure CNTs [20]. Unfortunately, SiCNTs composed of rolled-up graphene-like sheets, are also difficult to synthesize. Most synthetic methods produce either silicon carbide nanowires (SiCNWs) or biaxial $SiC|SiO_2$ nanowires instead. Synthesis of multi-walled SiCNTs, using CNTs as templates, was not achieved until recently [21].

Recent advances in computer technology and algorithm development have allowed theoretical calculations of the structures and properties of a wide variety of nanomaterials. Some of these methods, such as the density-functional theory (DFT), can treat very large molecules. Some studies use the so-called "cluster model"; yet others take advantage of the periodicities of the nanostructures. These calculations are of importance in that they provide a better understanding of the properties of these materials as well as allow predictions of the behavior of yet-unknown materials.

In this review, we focus on theoretical studies of silicon-based 1D nanomaterials. We shall begin with a short overview on the contrast of atomic properties of silicon vs. carbon, followed by theoretical studies of silicon nanowires (SiNWs), silicon nanotubes (SiNTs), crystalline silicon nanotubes (cSiNTs), silicon carbide nanowires (SiCNWs), silicon carbide nanotubes (SiCNTs), and other Si-based 1D nanomaterials. The acronyms of the various theoretical methods, along with a brief description of their applicabilities and limitations, are listed at the end for the sake of quick reference.

2. Atomic properties and bonding capabilities of silicon vs. carbon

Silicon, in comparison with carbon, has the following attributes: (1) lower electronegativity; (2) bonds involving silicon are, in general, weaker (except when bonded to very electronegative atoms); (3) kinetically more reactive; (4) larger atomic radius (which means larger orbital size and weaker π-type overlaps); (5) smaller energy difference between the valence *s* and the *p* orbitals, and hence lower hybridization energies; and (6) the availability of energetically low-lying *d* orbitals and the ability to expand its coordination sphere. These factors impact tremendously on the bonding capabilities and hence the chemical and physical properties of silicon, in comparison with those of carbon. We shall discuss each of these different attributes next.

First, the most important distinction between silicon and carbon is the difference in electronegativity (χ). In contrast to carbon ($\chi = 2.55$), silicon ($\chi = 1.90$) is less electronegative than hydrogen ($\chi = 2.20$). As a result, Si–H bonds are polarized in the opposite sense, as $Si^{\delta+}$–$H^{\delta-}$, instead of $C^{\delta-}$–$H^{\delta+}$. This implies that nucleophilic attacks on silanes usually occur at the silicon centers. Second, covalent bonds involving silicon are, in general, weaker by 25–75% when compared to those of carbon. For example, Si–H bonds are significantly weaker than C–H bonds, as indicated by their respective bond energies (318 kJ/mol for Si–H vs. 411 kJ/mol for C–H). The reverse is true when silicon is bonded to very electronegative atoms such as oxygen and halogens (X) due to the much higher ionic characters of the Si–O and Si–X bonds. Indeed, these latter bonds are very strong, with bond energies of 452 and 565, 381, 310 kJ/mol for Si–O and Si–X bonds where X = F, Cl, Br, respectively. In contrast, carbon bonded to electronegative atoms such as oxygen and halogens are weaker (C–O and C–X bond energies are 357.7 and 485, 327.2, 285 kJ/mol where X = F, Cl, Br, respectively). Third, silicon molecules are in general kinetically more reactive than the corresponding carbon molecules. For example, silanes are also much more reactive than the corresponding hydrocarbon analogs due to the greater polarization caused by the larger disparity in the electronegativities of silicon vs. its substituents. It is interesting to note the paradox that, Si–O and Si–X bonds, where the greatest bond polarization occurs, are thermodynamically stable (the second attribute) on the one hand and kinetically reactive (the third attribute) on the other hand, both owing to the very same reason of large bond polarization (i.e., with high ionic characters). Fourth, the larger atomic size of silicon gives rise to longer Si–Si

bonds of 2.35 Å and hence weaker Si–Si bonds with bond energy of 222 kJ/mol, in comparison to C–C bonds of 1.54 Å with bond energy of 345.6 kJ/mol. As a result of the poor π–π overlaps for silicon (smaller than those of carbon by roughly an order of magnitude), Si=Si bonds of 2.16 Å, with bond energy of 327 kJ/mol, are much weaker than C=C bonds of 1.34 Å with bond energy of 602 kJ/mol. Furthermore, more often than not, Si=Si bonds are non-planar (folded, twisted, or both) and Si≡Si bonds are nonlinear. In contrast, the small atomic size of carbon means efficient π–π overlap, and the formation of stable, planar double and linear triple bonds. The C–C, C=C, and C≡C bond lengths are 1.54, 1.34, and 1.20 Å, with bond energies of 345.6, 602, and 835.1 kJ/mol, respectively. Fifth, the energy difference between the valence *s* and *p* orbitals for silicon ($E_{3p} - E_{3s}$ = 5.66 eV) is only half of the corresponding value for carbon ($E_{2p} - E_{2s}$ = 10.60 eV). As a consequence, silicon tends to utilize all three of its valence *p* orbitals, resulting in sp^3 hybridization, in contrast to carbon which can "activate" one valence *p* orbital at a time (since hybridization costs energy), giving rise to *sp*, sp^2, and sp^3 hybridization schemes and the formation of triple, double, and single bonds, respectively, as required by the bonding situation. Finally, the *energetically* low-lying *d* or other virtual orbitals (such as the antibonding σ* orbitals) allow silicon to expand its coordination sphere from four to five or six. While this attribute greatly enriches the chemistry of silicon, it is detrimental to biological systems which rely on, among other things, the stability of chiral centers. In other words, the expansion of coordination spheres, especially in the case of fluxional behavior in solution, can cause racemization of the chiral centers. The energetically accessible *d*, π*, or σ* orbitals of silicon also allow "back bonding" to occur, with electron densities donated from the lone pair(s) of the bonded atom (substituent) back to the silicon virtual orbitals (thereby making them less basic) or the mixing of *d*-, π-, or σ-type orbitals. This bonding capability, which is not available to carbon, manifests itself in the reduced basicities of lone pairs of atoms (such as oxygen in siloxanes and nitrogen in silaxanes) attached to silicon. It is also one of the major causes of the non-planar structures of silenes and disilenes (often folded and sometimes twisted, or both), in addition to the weak π bonding indicated earlier.

In short, it is the peculiar properties of silicon, and its seemingly paradoxical contrasts with carbon, that make silicon chemistry and materials most interesting and useful.

3. Silicon nanowires (SiNWs): tuning of electronic structures and manipulations of properties

Experimentally, large quantities of SiNWs of different orientations have been synthesized using different methods, with controllable sizes and morphologies [22]. Theoretically, possible configurations of SiNWs enclosed by low-index crystal surfaces (some of which are shown in Fig. 1) have been investigated by density-functional tight-binding (DFTB) simulations [23]. For nanowires grown along <1 0 0>, <1 1 0>, and <1 1 1> directions, many low-index facet configurations and cross-sections are possible, making their controlled growth difficult. The <1 1 2> nanowires are the most attractive for research and applications because they have only one configuration of enclosing low-index facets with a rectangular cross-section, enclosed by two (1 1 1) and two (1 1 0) facets. (Note that {1 1 1} are the most stable and {1 1 0} are the next most stable facets.)

One of the major challenges toward SiNW-based photonic devices is the manipulation of the electronic band structure of the SiNWs to obtain a direct band-gap semiconductor. An indirect-to-direct band-gap transformation in <1 1 2>-oriented SiNWs can be induced by changing the cross-sectional size and shape of the nanowire, that is, changing the facets that enclose the nanowire

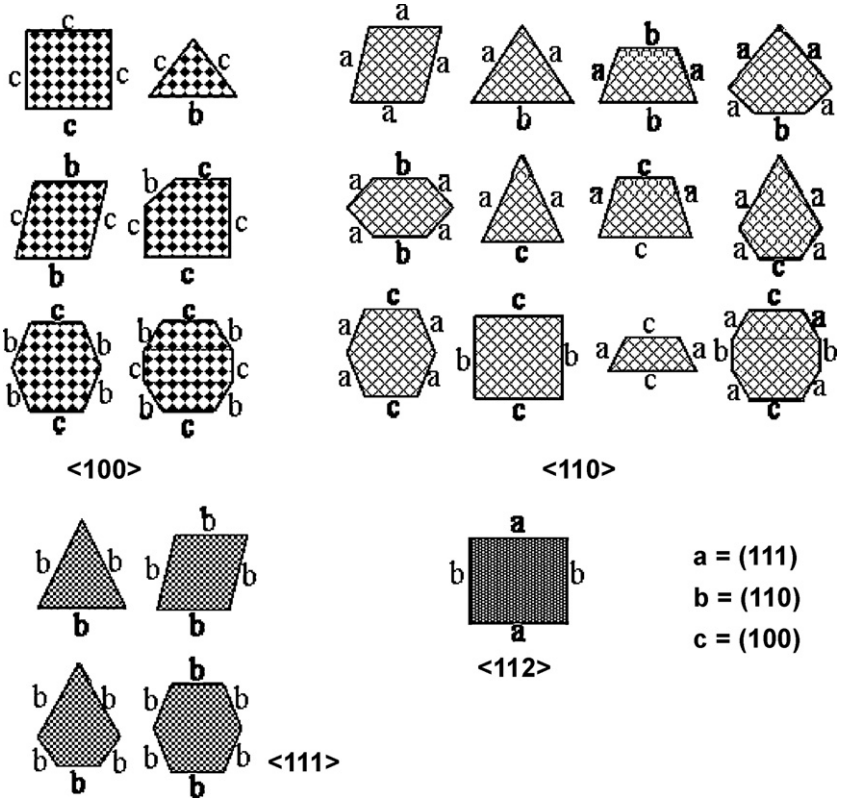

Fig. 1. Possible cross-sections of SiNWs grown along <1 0 0>, <1 1 0>, <1 1 1>, and <1 1 2> directions. Enclosing surfaces with symmetries lower than (1 0 0), (1 1 0), and (1 1 1) are excluded. For SiNWs grown along the <1 1 2> direction, only one cross-section enclosed by low-index surfaces is possible. (Reprinted with permission from Ref. [23]. Copyright 2005 American Institute of Physics.)

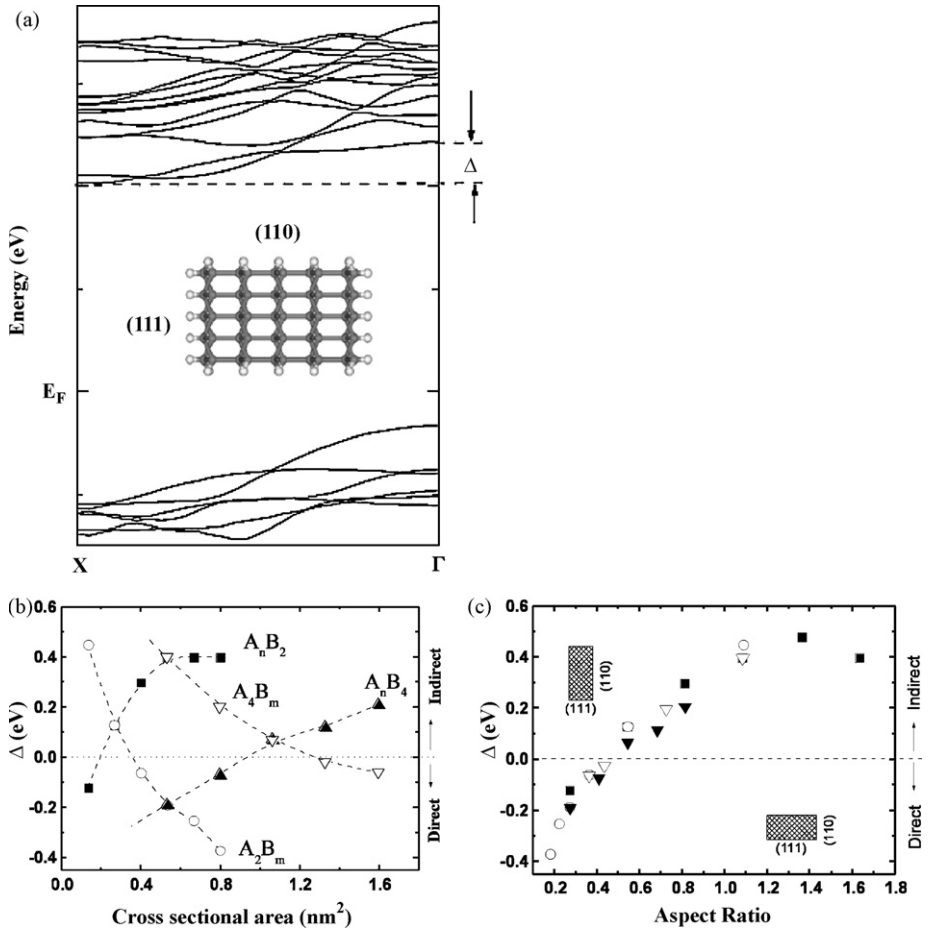

Fig. 2. (a) Band structure of a representative SiNW grown along the <1 1 2> direction with a cross-section A_4B_4. Here A_nB_m is used to distinguish the different cross-sections where A denotes the (1 1 1) facet and B the (1 1 0) facet. (b) Energy difference (Δ) vs. cross-sectional area of <1 1 2>-oriented SiNWs for four different series A_2B_m, A_4B_m, A_nB_2, and A_nB_4. The energy difference Δ is defined as the energy difference between the energy at the bottom of the conduction band at Γ and the energy minimum of the conduction band near X point shown in (a). (c) Δ vs. the aspect ratio measured in terms of the ratio of (1 1 1) to (1 1 0) facets. The two shaded rectangles (insets in (c)) are examples of cross-sections of <1 1 2>-oriented SiNW with different aspect ratios. The horizontal line in each figure at $\Delta = 0$ is the cross-over point from indirect (where $\Delta > 0$) band-gap to direct (where $\Delta < 0$) band-gap. (Reprinted with permission from Refs. [24,28]. Copyright 2008 American Institute of Physics and Institute of Physics (IOP).)

(see Fig. 2) [24]. Specifically, Fig. 2(a) portrays the band structure of a representative SiNW grown along the <1 1 2> direction with a cross-section A_4B_4. Here A_nB_m is used to distinguish the different cross-sections where A denotes the (1 1 1) facet and B the (1 1 0) facet. Fig. 2(b) shows the energy difference (Δ) vs. cross-sectional area of the SiNWs for four different series A_2B_m, A_4B_m, A_nB_2, and A_nB_4. Here Δ is defined as the energy difference between the energy at the bottom of the conduction band at Γ and the energy minimum of the conduction band near X point shown in Fig. 2(a). Finally, Fig. 2(c) depicts the effect of the aspect ratio, measured in terms of the ratio of (1 1 1) to (1 1 0) facets, on the energy difference Δ. The two shaded rectangles (insets in (c)) are examples of cross-sections of SiNWs with different aspect ratios. The horizontal line in each figure at $\Delta = 0$ is the cross-over point from indirect (where $\Delta > 0$) band-gap to direct (where $\Delta < 0$) band-gap. It can be seen from Fig. 2 (b) and (c) that an indirect band-gap <1 1 2>-oriented SiNW can be transformed into a direct band-gap SiNW by manipulating its cross-sectional area and shape (in this case the aspect ratio of a rectangular cross-section).

In addition, the axial stress along the growth direction, which depends on the crystal orientation and the diameter of the SiNWs, can modulate the band structure and induce the indirect-to-direct band-gap transition [25,26]. Also, adsorption of heteroatom such as phosphorus on the surface of SiNWs can cause a change in the local density of states (LDOS) near the Fermi level and induce the indirect-to-direct band-gap transition as well [27].

Band-gap tuning is important in Si-based visible optical devices. The band structure of SiNWs around the Fermi level is strongly influenced by variables such as the nanowire diameter, the growth orientation, morphology, as well as by the chemical properties of the passivating shell [29]. Vo et al. have shown that the band-gap of SiNWs decreases with increasing diameter and can be further reduced by surface reconstruction [30]. Rurali and Lorente employed density-functional theory to analyze SiNWs grown along the <1 0 0> direction [31,32]. They found that the electronic structure behavior is dictated by the surface states of the reconstruction. In particular, two energy-equivalent surface reconstructions prevailed, one was strongly metallic while the other one is semimetallic.

Replacement of surface silicon atoms (hereafter referred to as "surface doping") by foreign atoms can also result in metallization of the SiNWs. For example, metallization can be induced by "surface doping" with nitrogen atoms on SiNWs (replacing some of surface silicon atoms at certain key positions) [33]. As depicted in Fig. 3, the partial density of states (PDOS) of surface silicon atoms on the (1 1 0) vs. <1 0 0> facets of SiNWs grown along <1 1 0> direction revealed an increase in the density of states of both at the Fermi level. This is attributable to the Si–N orbital interactions on the respective surface. However, the increase is significantly greater in the case of the nitrogen "surface doping" on the (1 1 0) facets which can be traced to the energetically favorable zigzag Si–N chain on the (1 1 0) facet, thereby giving rise to metallic states near the Fermi

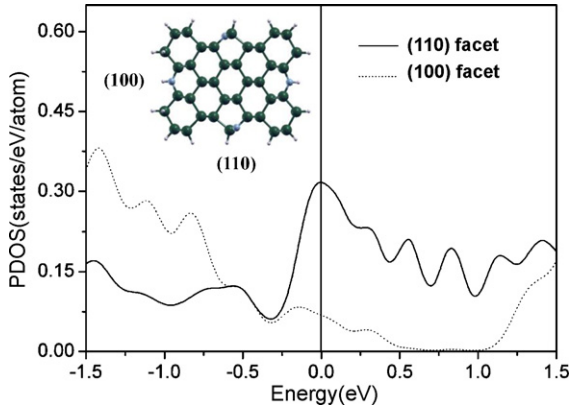

Fig. 3. Partial density of states (PDOS) of surface silicon atoms of SiNWs grown along <1 1 0> direction with nitrogen adsorption (Si:N = 38:4). The inset represents a cross-section of the nanowire, enclosed by two (1 0 0) and two (1 1 0) facets. The solid line shows the PDOS for the silicon atom in the (1 1 0) facet and the dotted line for the silicon atom in the (1 0 0) facet. The Fermi level is set at zero. Silicon and nitrogen atoms are represented by dark and light spheres while hydrogen atoms are represented by the smallest spheres. (Reprinted with permission from Ref. [33]. Copyright 2009 American Institute of Physics.)

level. The PDOS examination showed that the *p* orbitals of surface Si atom are modified by the N atom.

The effect of doping with impurities on the conductivity of SiNWs was also studied via DFT calculations [34]. It was found that impurity surface segregation strongly affects the conductance associated with surface states in the case of unpassivated nanowires. Upon passivation, the large surface to bulk aspect ratio of SiNWs is expected to lead to the neutralization by surface defects of impurities up to a large critical concentration below which the conductivity will not raise rapidly with doping. The different behavior of P versus B doping indicates that *n*-type or *p*-type doping may lead to significantly different conducting properties in the nanowires as compared to the bulk phase.

The electronic properties of different-sized SiNWs with different surface coverage (H, Br, Cl, and I) have been investigated by DFT calculations [35]. The surface chemistry was shown to have strong effects on the band structure of SiNWs, comparable to that of quantum confinement. The primary cause of the band-gap change is the suppression of surface states as determined by the strength of the surface bonds. In another study, the effects of surface modification of SiNWs grown along various directions by hydroxyl and fluoro groups on the band structure have also been explored by a multi-scale approach that combines geometry optimization using the semi-empirical AM1 method and DFT band structure calculation using the BPW91 functionals [36]. Surface modification of the SiNWs using these functional groups can strongly reduce the band-gap by as much as 1 eV, and more interestingly, alter the gap nature. Moreover, SiNWs of different orientations exhibit different degrees of band-gap reduction upon surface modification, in which the <1 1 0> SiNW demonstrates the highest sensitivity. The result indicates that SiNWs grown along the <1 1 0> direction are the better candidate for sensor application. On the contrary, the <1 1 0> SiNWs exhibiting different cross-sectional patterns do not show significant differences in their band-gaps, indicating that the electronic structures of SiNWs are much more sensitive to surface modification than the change of cross-section. In contrast, the <1 1 1>-oriented SiNWs are structurally more stable and less sensitive to surface modification. Finally, the electrical conductivity of the SiNWs is highly sensitive to surface modification.

The electronic properties of SiNWs can also be modified by doping for the purpose of optoelectronic applications. The atomic and electronic structures of hydrogen saturated SiNWs doped with impurity atoms (such as Al, Ga, C, Si, Ge, N, P, As, Te, Pt) have been investigated using a first-principle plane wave method [37]. All impurities studied lead to a nonmagnetic ground state with a significant binding energy. Impurity bands formed at high impurity concentration are metallic for group IIIA and VA elements but are semiconductor for group IVA and VIA elements. While low substitutional impurity concentration leads to the usual *n*- and *p*-type behavior reminiscent of bulk silicon, this behavior is absent if the impurity atom is adsorbed on the surface. Functionalization of SiNWs with transition metal atoms has also been investigated by first-principle calculations [38,39]. Durgun et al. [38] investigated the energetics of adsorption and resulting electronic and magnetic properties of SiNWs surface-doped with different 3*d*-TM atoms at different levels. In general, "surface doping" of TM atoms results in a magnetic ground state. The net magnetic moment increases with increasing level of doping. At low coverage, the SiNWs may acquire half-metallic behavior, which means that they are insulators for one spin direction, but show metallic properties for the opposite spin direction. At high coverage, the ferromagnetic SiNWs become metallic for both spin directions, and some of them have very high spin polarization at the Fermi level. Thus, the spin-dependent electronic properties can be engineered by changing the type of TM atoms, as well as the diameter of the nanowire. It was suggested by these authors that the electronic and spintronic devices with conducting interconnects between them can be fabricated on a single SiNW at a desired order.

Under typical growth conditions, NWs are often observed to be tapered [40,41] by as much as 1 nm in diameter for every 10 nm in length. Structural tapering of SiNWs has been shown to have a profound effect on their electronic properties by *ab initio* calculations [42]. In particular, the electronic structure of small-diameter tapered SiNWs have a strong axial dependence, with unoccupied eigenstates being substantially more sensitive to diameter. Moreover, the states corresponding to the highest occupied and the lowest unoccupied states are spatially separated along the wire axis by the tapering-induced charge transfer and a strong electrostatic potential gradient, due to an appreciable variation in quantum confinement strength with diameter.

Extensive *ab initio* studies aimed at searching for stable geometries of <1 0 0> SiNWs [43] revealed that there are magic numbers for NWs. Extraordinarily high piezoresistance coefficients in a pristine <1 1 1> SiNW were found through systematic first-principle calculations [44]. This phenomenon stems from the interplay between two surface states with different localizations and unusual surface relaxation. Lattice compression along the growth axis causes a switch between light and heavy surface states and, consequently, alters the effective masses of carriers [45].

4. Silicon nanotubes (SiNTs): the Knowns and the Yet Unknowns

As discussed in Section 2, unlike carbon, silicon favors the sp^3 hybridization, and tends to form SiNWs rather than SiNTs. This is consistent with the calculated high formation energies of the SWCNT-like SWSiNTs [46] or the rolled-up Si (1 1 1) sheets [47] in comparison to the bulk silicon with diamond structure. We shall call these sp^2 SiNTs. Thus, unlike CNTs, the analogous silicon nanotubes, based on rolled-up graphene-like sheets, have not been made, despite several experimental claims to the contrary. Nevertheless, several theoretical investigations have suggested the possibility of their existence and predicted their structures and properties [46–50].

A related type of silicon nanostructure, described as crystalline silicon nanotubes, cSiNTs, has recently been prepared [51–55].

Table 1
The degree of distortion of silicon nanotubes as a function of the idealized hybridizations of the Si–Si bond, producing various possible structures. (Reprinted with permission from Ref. [47]. Copyright 2005 American Chemical Society.).

Structure types	Smooth CNT-like tube	Gear-like puckering	String-bean-like distortion	Severe distortion	Collapsed tube
Degree of distortion	→				
Structural feature			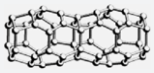		
Si–Si bond hybridization	sp^2–sp^2	sp^2–sp^3	sp^2–sp^3	sp^3–sp^3	sp^3–sp^3

However, these latter nanostructures, to be discussed in Section 4.3, are best considered as crystalline silicon nanopipes or hollow crystalline silicon nanowires or nanorods. We shall call these sp^3 SiNTs. (We should note here that there was a recent report on the fabrication of ultrathin "SiNTs" with a puckered structure [56]. However, the dependence of the electronic structure on the tube chirality revealed in that experiment is inconsistent with the theoretical prediction based on cylindrical SWSiNTs. Thus, these ultrathin "SiNTs" are best described as cSiNTs.)

It should be cautioned that the terms sp^2 and sp^3 are used loosely here to represent trigonal and tetrahedral coordination, respectively. As we shall see in the next subsections, local sp^2 coordination of silicon can either be planar or non-planar, owing to the peculiar atomic properties of silicon described in Section 2. In the latter case, the bond angles can approach that of the tetrahedral coordination expected of the sp^3 hybridization.

4.1. The sp^2 SiNTs

There were several claims of the synthesis of multi-walled sp^2 SiNTs. However, the reported experimental evidence were reviewed critically by Perepichka and Rosei [57] and shown to be inconclusive. In particular, of the four experimental reports on SiNTs reviewed by Perepichka and Rosei, "none of them describes a realistic model for the growth process and overall properties of these novel one-dimensional systems, and there is limited agreement with previous theoretical predictions." Furthermore, these latter authors showed that the microscopic images and the spectroscopic evidence, along with the chemical and physical properties, do not support the characterization of the products as sp^2 SiNTs. They further concluded that "the structure of SiNTs is still an open question of fundamental physical and chemical importance, which clearly requires concerted efforts between theoreticians and experimentalists."

Nonetheless, there is no doubt that CNT-like sp^2 SiNTs will be synthesized in due course. In the meantime, theoretical calculations can provide some insights regarding the structures and properties of these yet-to-be-prepared silicon nanostructures. We shall highlight some of these recent reports in the following subsections. Hopefully these results will inspire experimentalists to pursue novel synthetic routes to these elusive nanomaterials.

4.1.1. Single-walled sp^2 SiNTs

Based on silicon's "disinclination" to adopt the sp^2 coordination, Seifert et al. [58] argued that the existence of SiNTs is doubtful. Alternatively, these authors proposed that Si-based silicide and SiH nanotubes are theoretically stable and energetically viable, and could thus be considered as sources of SiNTs, particularly in view of the existence of many layered silicides. On the other hand, by applying DFT, Fagan et al. [48] investigated the similarities between silicon and carbon nanotubes. Their results showed that the electronic and structural properties of SiNTs are similar to those of CNTs, i.e., they may exhibit metallic or semiconducting behaviors, depending on the structure type (zigzag, armchair, or chiral) and the tube diameter. The strain energies of such structures have recently been described by Barnard and Russo [49]. Later, Kang et al. performed classical molecular dynamics (MD) simulations for hypothetical SiNTs using the Tersoff potential. They investigated the thermal behavior of hypothetical SiNTs and the difficulty in producing SiNTs or graphite-like sheets [59]. We shall describe two theoretically predicted structures of SiNTs in the following subsections.

4.1.1.1. String-bean-like SiNT structures. In a recent publication [50], Zhang et al. compared the electronic structures of four systems: a diamond-structured carbon nanowire (CNW), a SiNW, a CNT, and a SiNT in order to elucidate the differences in the structures and bonding between cubic (diamond-like) and tubular nanostructures of carbon and silicon with the hope of understanding the reason(s) for the hitherto unsuccessful synthesis of the silicon analogs of the CNTs.

Fig. 4 shows the four model compounds studied in this work. They represent a diamond nanowire, $C_{54}H_{60}$ (**1**), a silicon nanowire, $Si_{54}H_{60}$ (**2**), a carbon nanotube, $C_{54}H_{12}$ (**3**), and a silicon nanotube, $Si_{54}H_{12}$ (**4**). The carbon nanotube selected here has an armchair (3,3) structure. It is one of the smallest carbon nanotubes reported recently [60–62]. Hydrogen atoms were added to saturate the dangling bonds. PM3 parametrization [63] of the MNDO semi-empirical Hamiltonian [64] was used. The results were further substantiated by *ab initio* calculations.

For the geometrically optimized nanostructures **1**–**4**, there are general trends of bond length variations. As indicated in Fig. 4, the C–C bonds in structure **1** are about 1.54 Å, as expected for single bonds. Similarly, the Si–Si bonds in structure **2** average about 2.35 Å, also expected for single bonds. In the CNT **3**, the C–C bond lengths alternate between 1.40 and 1.46 Å, indicating a relatively small degree of C=C vs. C–C bond localization. In other words, the small bond length alternation of about 0.06 Å signifies that π delocalization is extensive in CNTs. SiNT such as **4** also shows similar bond length alternation (see Fig. 4), but with a much larger variation of 0.40 Å. The shortest Si–Si bond length is only about 1.85 Å, while the longest is about 2.25 Å, showing a stronger tendency for bond localization (Si=Si vs. Si–Si). As can be seen from Fig. 4, the CNT **3** has a smooth surface and a more-or-less uniform tube diameter. In contrast, the SiNT **4** has a puckered (corrugated) structure which may be referred to as the "string-bean" distortion. It has a periodically varying diameter.

A detailed analysis of the total density of states revealed that tubular structures for silicon are, in general, less stable and tend to relax to the diamond-like structure with tetrahedral configuration, which allows for the largest extent of overlap of the sp^3-hybridized orbitals. The results also suggest that SiNTs are less stable than the corresponding CNTs; the cause of which can be traced to the differences in the energetics and overlaps of the valence *s* and *p* orbitals of C vs. Si discussed earlier. In particular, the poor π–π overlap of silicon weakens the π delocalization and under appropriate conditions, may lead to a puckered tubular structure as exemplified by the armchair structure **4**.

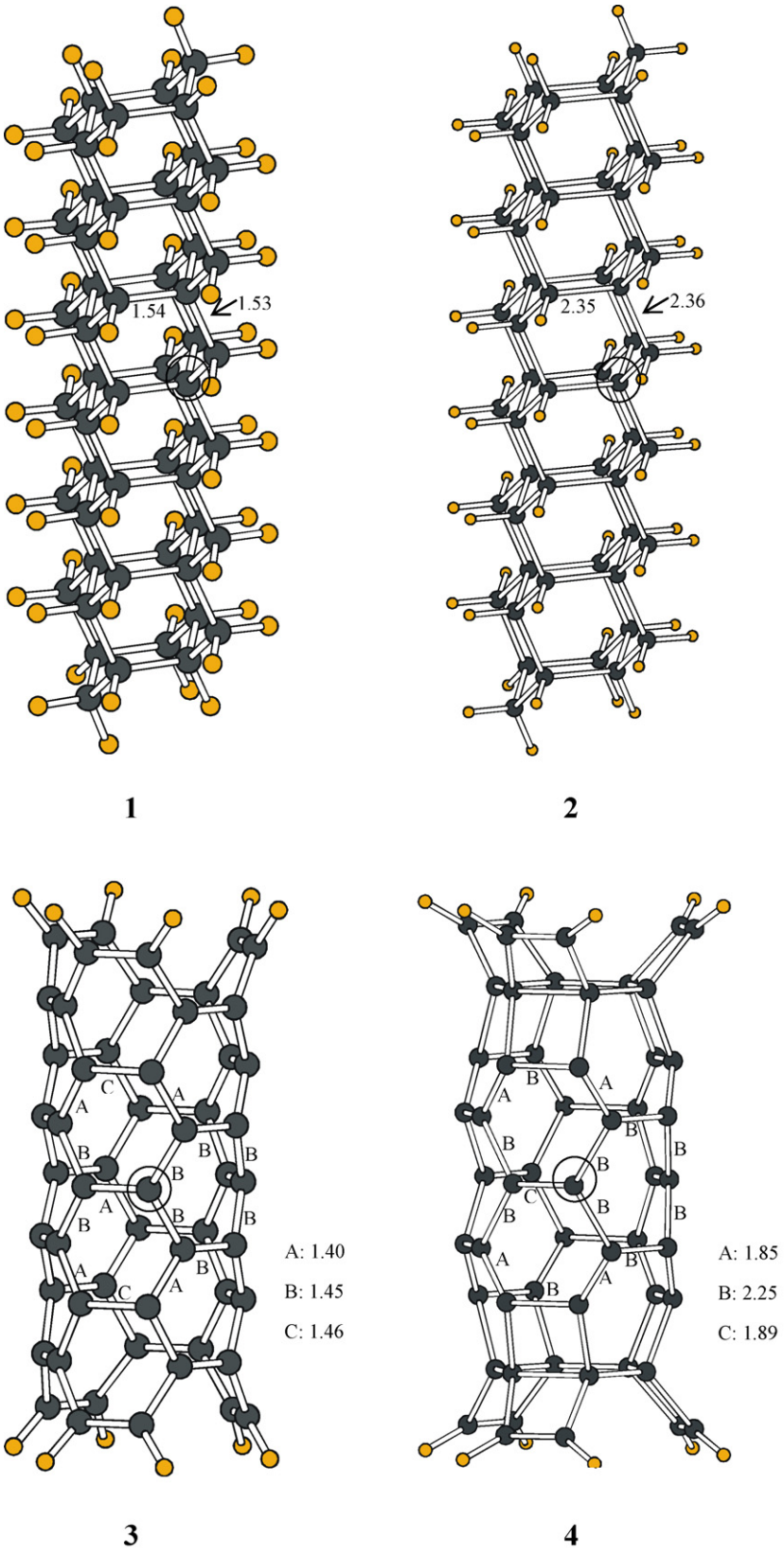

Fig. 4. Four model compounds: a diamond nanowire $C_{54}H_{60}$ (**1**), a silicon nanowire $Si_{54}H_{60}$ (**2**), a carbon nanotube $C_{54}H_{12}$ (**3**), and a silicon nanotube $Si_{54}H_{12}$ (**4**). (Reprinted with permission from Ref. [50]. Copyright 2002, with permission from Elsevier.)

4.1.1.2. Gear-like SiNT structures. In a follow-up publication [47], Zhang et al. explored the structural and energetic characteristics of different types (zigzag, armchair, and chiral) of SiNT structures by performing density-functional molecular dynamics simulations at various temperatures. A number of the findings were subsequently substantiated by *ab initio* Hartree-Fock (HF) or DFT calculations.

Single-walled SiNTs can adopt a number of distorted tubular structures (see Table 1), representing respective local energy minima, depending on the theory used and the initial model adopted. In particular, "gear-like" structures containing alternating sp^3-like and sp^2-like silicon local configurations were found to be the dominant structural form for SiNTs via extensive density-functional tight-binding molecular dynamics (DFTB-MD) simulations (followed by geometrical optimization using HF or DFT) at moderate temperatures (below 100 K). The gear-like structures of SiNTs deviate considerably from, and are energetically more stable than, the smooth-walled tubes (the silicon analogs of single-walled carbon nanotubes (SWCNTs)). The energetics and the structures of gear-like SiNTs are shown to depend primarily on the diameter of the tube, irrespective of the type (zigzag, armchair, or chiral). In contrast, the energy gap is very sensitive to both the diameter and the type of the nanotube.

The temperature dependence of the structure of SWSiNTs was probed by DFTB-MD calculations. At 0 K, SiNTs deviate only slightly from the smooth-walled structures analogous to those of CNTs. However, as the temperature was raised to 10–30 K, considerable structural deformation can occur. Further annealing at higher temperatures eventually led to the collapse of many of the SiNTs. As a general rule, small-diameter zigzag (n, 0) SiNTs (for $n < 6$) easily collapse in the temperature range of 10–30 K, while SiNTs with larger diameters can withstand higher temperatures in the annealing process.

The annealed SiNTs contain two alternating silicon sites, "A" and "B." Site "A" is close to tetrahedral while site "B" is more-or-less trigonal planar, as indicated by the sums of bond angles, $\Sigma\alpha$ and $\Sigma\beta$, where $\Sigma\alpha$ and $\Sigma\beta$ designate the sums of the three angles around site "A" and site "B" silicon atoms (see Fig. 5), respectively. Fig. 6 shows the variation of $\Sigma\alpha$ and $\Sigma\beta$ as functions of the tube diameter. A sum close to the ideal value of $3 \times 109.47^\circ = 328.4^\circ$ is taken here as an indication of a tetrahedral structure (with sp^3-like hybridization), whereas a sum close to the ideal value of $3 \times 12^\circ = 360^\circ$ is indicative of a trigonal planar structure (with sp^2-like hybridization). It can be seen from Fig. 6 that $\Sigma\alpha$ and $\Sigma\beta$ are generally independent of the type or chirality of the SiNTs. They are, however, highly dependent on the diameter of the tube.

Fig. 7 shows the variation of cohesive energies of the relaxed "gear-like" SiNTs as a function of the diameter of the tube. The cohesive energy varies linearly with the inverse of the tube diameter, regardless of the type (zigzag, armchair, or chiral) of the SiNT. The cohesive energy approaches asymptotically a value of about 4.77 eV per silicon atom as the diameter increases. A similar relationship between cohesive energy and tube diameter was also observed for CNTs [48].

In sharp contrast, the calculated energy gaps (see Fig. 8) seem to depend critically on the type or chirality of the tube. They are all semiconductors with small band-gaps (<1 eV), leveling off to fractions of an eV at large diameters. Only those of the armchair (n,n) SiNTs show a linear relation to the inverse of the diameter of the tube. For the purpose of comparison, SWCNTs can either be metallic or semiconducting. All armchair SWCNTs are metals; those with $n - m = 3k$, where k is a nonzero integer, are semiconductors with a small band-gap; and all others are semiconductors with a band-gap which is inversely proportional to the nanotube diameter [12]. Within the limited set of zigzag SiNTs calculated, the $n - m = 3k$ anomaly also seems to occur, i.e., the band-gaps of zigzag (n,0) SiNTs where $n = 3k$ are abnormally small (cf. Fig. 8).

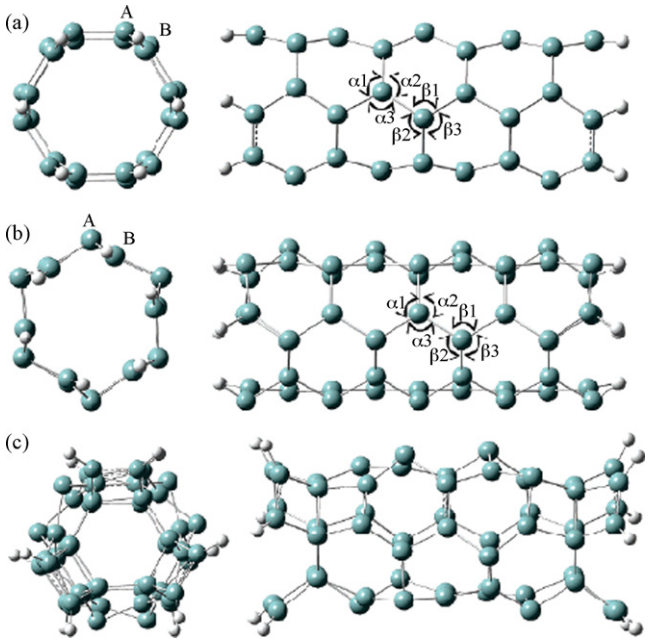

Fig. 5. Optimization of the structure of the armchair (3,3) SiNT with *ab initio* calculations at the HF/6-31G(d) level starting with the structures of (a) a smooth tube analogous to CNT, (b) the gear-like configuration obtained by performing MD, and (c) string-bean-like puckering obtained by using PM3. (Reprinted with permission from Ref. [47]. Copyright 2005 American Chemical Society.)

Table 1 shows schematically the structural features and the extents of distortion of the various possible structures of SiNTs. The CNT-like structure is that of a smooth tubular shape and represents a local energy minimum for a given type of silicon nanotube. It contains mostly sp^2–sp^2 Si–Si bonding. The gear-like structure is that of a deformed tubular shape and represents an energetically more favorable local minimum. The wave-like deformation of the circumference of the cross-section gives rise to the gear-like shape. It is of good structural order containing mostly sp^2–sp^3 Si–Si bonding. The string-bean-like structure involves more distortion. The puckering is along the tube axis, containing mostly sp^2–sp^3 Si–Si bonding. Progressively more severe distortion results in the disruption of the tubular structure, though it may be energetically more favorable because of the increased number of sp^3–sp^3 Si–Si

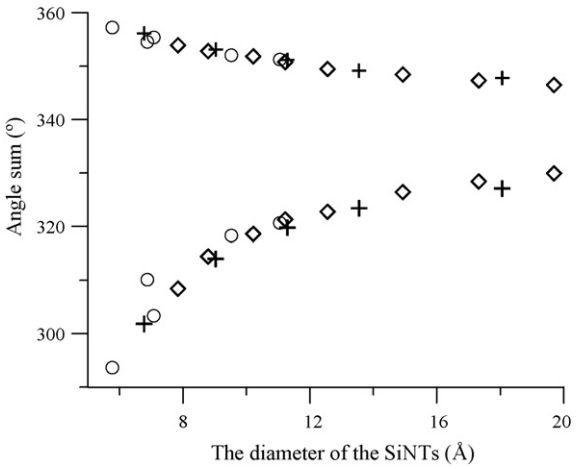

Fig. 6. Sums of bond angles $\Sigma\alpha$ (=$\alpha1 + \alpha2 + \alpha3$) and $\Sigma\beta$ (=$\beta1 + \beta2 + \beta3$) vs. the diameter of the SiNTs. The data points are "(◊)" for zigzag (n,0), "(+)" for armchair (n,n), and "(○)" for chiral (n,m) SiNTs. (Reprinted with permission from Ref. [47]. Copyright 2005 American Chemical Society.)

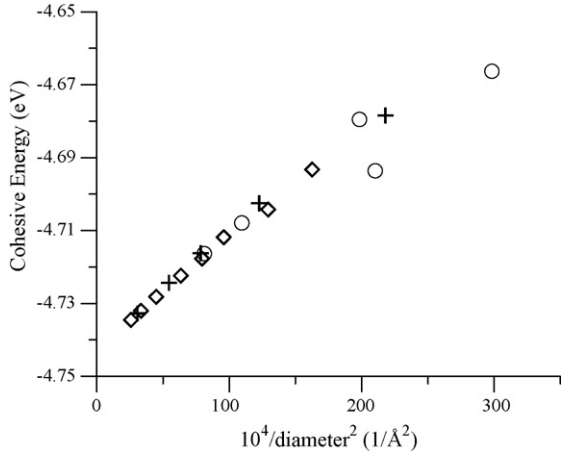

Fig. 7. Cohesive energy vs. 10^4/diameter^2 for the SiNTs. The data points are "(◊)" for zigzag (n,0), "(+)" for armchair (n,n), and "(○)" for chiral (n,m) SiNTs. (Reprinted with permission from Ref. [47]. Copyright 2005 American Chemical Society.)

bonding. Final total collapse of the tube might occur when the distortion becomes so severe that the structure no longer looks like a tube but rather resembles that of amorphous sp^3 silicon.

4.1.2. Double-walled sp^2 SiNTs

MD simulations based on an empirical force field as well as first-principle calculations have shown that double-walled SiNTs built analogous to CNTs are energetically unstable, undergoing considerable structural distortion towards amorphous-like SiNTs by the formation of a large number of sp^3 bonds especially at high temperatures [65].

4.1.3. Predictions of the structures and properties of sp^2 SiNTs

While the calculated structures of SiNTs may be sensitive to the method used, several general predictions can be made. First, the weak π–π overlap in Si=Si bonds, even in near-planar structures, generally implies relatively weak silicon double bonds. Consequently, silenes and disilenes are usually synthesized with (and stabilized by) bulky ligands. They are often non-planar, folded and/or twisted to a varying degree. These attributes, carried over to SiNTs, would mean severe *structural distortion* and *thermodynamic instability*. Second, though the mode of distortions may take on a variety of forms, and vary from system to system, it will most likely involve a combination of, or more appropriately, a compromise between, sp^3-like and sp^2-like local silicon configurations. Third, since the sum of the energies of two single Si–Si bonds is greater than that of a double Si=Si bond, there is a tendency for two Si=Si bonds to couple (via [2+2] interaction), giving rise to four single bonds. This property will probably carry over to the SiNTs. In this context, the tendency of SiNTs to distort, and eventually collapse at high enough temperatures, may also be traced to the formation of Si–Si bonds in place of the Si=Si bonds. Obviously this tendency to convert sp^2- to sp^3-hybridized silicon via [2+2] coupling becomes more pronounced between layers of silicon in multi-walled SiNTs. Finally, SiNTs, like molecular silicon compounds, will probably be more reactive than their CNT analogs in the sense that they are *kinetically labile*. Generally speaking, this kinetically lability is caused by the many reaction pathways with low activation energies available to silicon (in contrast to carbon) as a result of the smaller energy gap between HOMO and LUMO (as well as the energy difference between these frontier MOs and the Fermi level) and the availability and energetic accessibility of virtual *d* orbitals in the case of silicon.

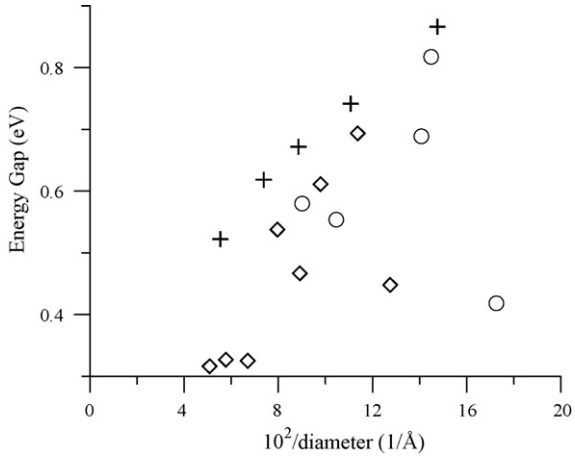

Fig. 8. Energy gap vs. the 10^2/diameter for the SiNTs. The data points are "(◊)" for zigzag (n,0), "(+)" for armchair (n,n), and "(○)" for chiral (n,m) SiNTs. (Reprinted with permission from Ref. [47]. Copyright 2005 American Chemical Society.)

It is well known that disilenes have $\pi \rightarrow \pi^*$ transitions with approximately half the energy of that of the carbon analogs. Because of this relatively small HOMO–LUMO gap (ca. 3 eV), disilenes oxidize at less positive potentials and reduce at less negative potentials than the corresponding alkenes. Also, disilenes are both better Lewis π bases and better Lewis π acids than the corresponding alkenes. We expect SiNTs to inherit most, if not all, of these attributes. For example, we expect SiNTs to exhibit interesting optical properties (due to the participation of energetically low-lying virtual *d* orbitals) and lower-energy transitions (in comparison to the corresponding CNTs). They should also be easier to both oxidize and reduce, and should behave as better π donors and better π acceptors, than their carbon analogs.

4.2. The sp^3 SiNTs

4.2.1. Single-walled sp^3 SiNTs

The hybridizational orientation-induced activity of Si dangling bonds can be efficiently passivated by foreign charges, atoms or groups. A model based on tetragons of sp^3-hybridized silicon atoms (with additional electrons or H saturated) has been proposed using density-functional tight-binding theory (DFTB) [66]. This model is particularly intriguing since the fragments of this structure are known as stable molecules (in contrast to fragments of sp^2 SiNTs, for example, the hypothetical hexasilabenzene).

It is known that layered silicon systems exist in some silicides. For instance, in alkaline-earth metal silicides [67], the silicon layers, formed by cyclohexane-like rings, are separated by metal ions. It is conceivable that the layered structure of silicon in these systems could be rolled-up to form tubular structures analogous to the "gear-like" configurations described earlier. Indeed, using first-principle DFT calculations, Singh et al. [66,68] showed that hexagonal metallic silicon nanotubes can be stabilized by doping with Be or 3*d*-TM atoms (Figs. 9 and 10). The resulting nanostructures are more stable than those formed from elemental silicon. Their electrical, magnetic and optical properties can be modified by changing the metal atoms. Finite nanotubes doped with Fe and Mn have high local magnetic moments, whereas Co-doped nanotubes have low values and Ni-doped nanotubes are mostly nonmagnetic. The infinite $Si_{24}Fe_4$ nanotube (Fig. 11) is ferromagnetic with nearly the same local magnetic moment on each Fe atom as in bulk iron. Mn-doped nanotubes are antiferromagnetic, but a ferromagnetic state lies only 0.03 eV higher in energy with a gap in the majority spin bands near the Fermi energy. These materials are potentially useful for silicon-based spintronic devices and other nanoscale magnetic applications.

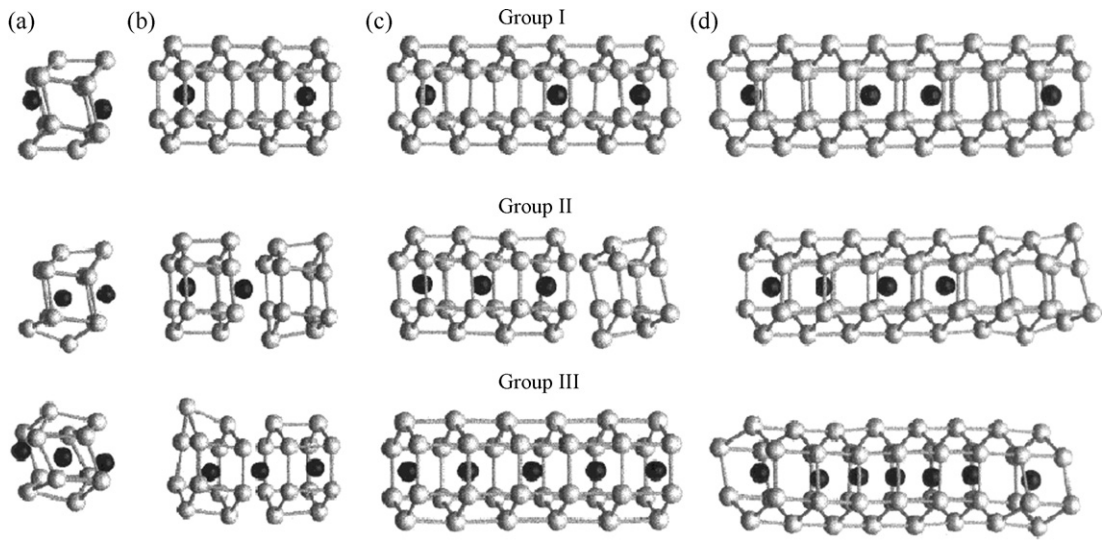

Fig. 9. Finite doped Si nanostructures: (a) $Si_{12}Be_x$ (x = 2 and 3), (b) $Si_{24}Be_x$ (x = 2 and 3), (c) $Si_{36}Be_x$ (x = 3 and 5), and (d) $Si_{48}Be_x$ (x = 4 and 7). Groups I and II represent structures with the same number of Si and Be atoms but different distributions of Be atoms, while the structures in group III have higher concentrations of Be atoms. (Reprinted with permission from Ref. [66]. Copyright 2002 American Chemical Society.)

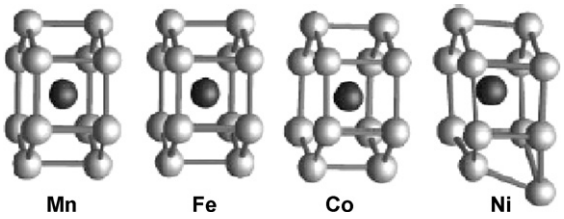

Fig. 10. Lowest energy structures of the finite nanotubes with stoichiometry $Si_{12}M$ (M = Mn, Fe, Co, and Ni). (Reprinted with permission from Ref. [68] (http://link.aps.org/abstract/PRL/v91/p146802). Copyright 2003 by the American Physical Society.)

Using *ab initio* calculations, Dumitrica et al. [69] showed how the smallest (2,2) and (3,0) silicon nanotubes can be stabilized by the axially placed metal atoms (such as Be, Ca, Sc, Ti, Cr, and Zr) to form nearly one-dimensional metal silicide nanowires with substantial cohesive energy, mechanical stiffness, and metallic density of states.

Durgun et al. [70] showed that (n,0) zigzag and (n,n) armchair nanotubes of silicon having $n \geq 6$ are stable while those with $n < 6$ are unstable. The latter, however, can be stabilized by internal or external adsorption of transition metal elements (e.g., V, Ti, Cr). Some of these tubes have a magnetic ground state leading to spintronic properties. Zhao and coworkers [71] found the incorporation of Co atoms into the wall of SiNTs not only effectively stabilizes the tubes but also tunes their electronic properties. The electronic structures of $CoSi_2$NTs display metallic characteristics.

Table 2
The diameter (d), formation energy (ΔE_{form}), and energy band-gap (E_{gap}) of select SiO nanotubes. The diameters are in angstroms. The formation energies are in eV/atom, and the energy band-gaps are in eV. (Reprinted with permission from Ref. [72]. Copyright 2007 American Institute of Physics.).

(n_1:n_2)	d	ΔE_{form}	E_{gap}
(5:0)	6.07	0.54	0.91
(12:0)	11.43	0.65	1.37
(6:6)	11.44	0.59	0.22
(8:4)	10.91	0.51	0.95
(9:3)	11.46	0.50	0.63
(10:5)	12.20	0.49	0.74
(8:8)	13.90	0.54	0.14
(12:4)	13.71	0.51	0.49
(9:9)	15.07	0.52	0.17
(12:6)	14.59	0.49	0.84

In one study, Zhao et al. [72] suggested an interesting route to stabilize SiNTs by incorporating oxygen atoms, thereby tuning their electronic properties. In this case, SiO nanotubes (SiONTs) were built by stacking silicon dodecagons bridged by oxygen atoms. Four representative (n_1:n_2) isomers (namely (12,0), (6,6), (8,4), and (9,3)) of the resulting SiO nanotubes are depicted in Fig. 12. Here (n_1:n_2) denotes the numbers of the exterior and the interior oxygen atoms, respectively. Table 2 shows the diameter, formation energy (ΔE_{form}), and energy band-gap (E_{gap}) of select SiO nanotubes. Among the four isomers shown in Fig. 12, (12:0) SiONT is energetically most unfavorable. The (8:4) and (9:3) SiONTs are energetically comparable, and both are more stable than the (5:0) SiONT by about 0.03 and 0.04 eV/atom, respectively. All the SiONTs

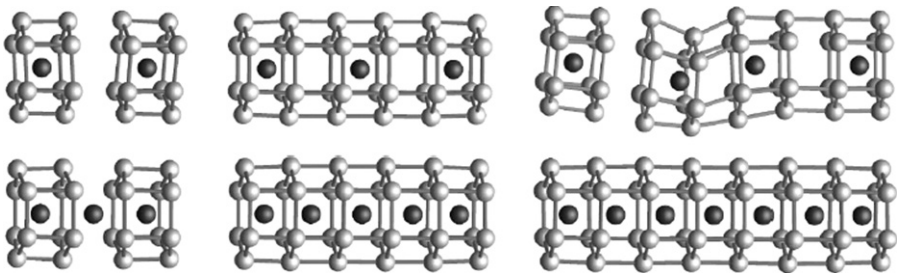

Fig. 11. Structures of Fe-doped finite silicon nanotubes with stoichiometries $Si_{24}Fe_2$, $Si_{36}Fe_3$, $Si_{48}Fe_4$, $Si_{24}Fe_3$, $Si_{36}Fe_5$, and $Si_{48}Fe_7$. (Reprinted with permission from Ref. [68] (http://link.aps.org/abstract/PRL/v91/p146802). Copyright 2003 by the American Physical Society.)

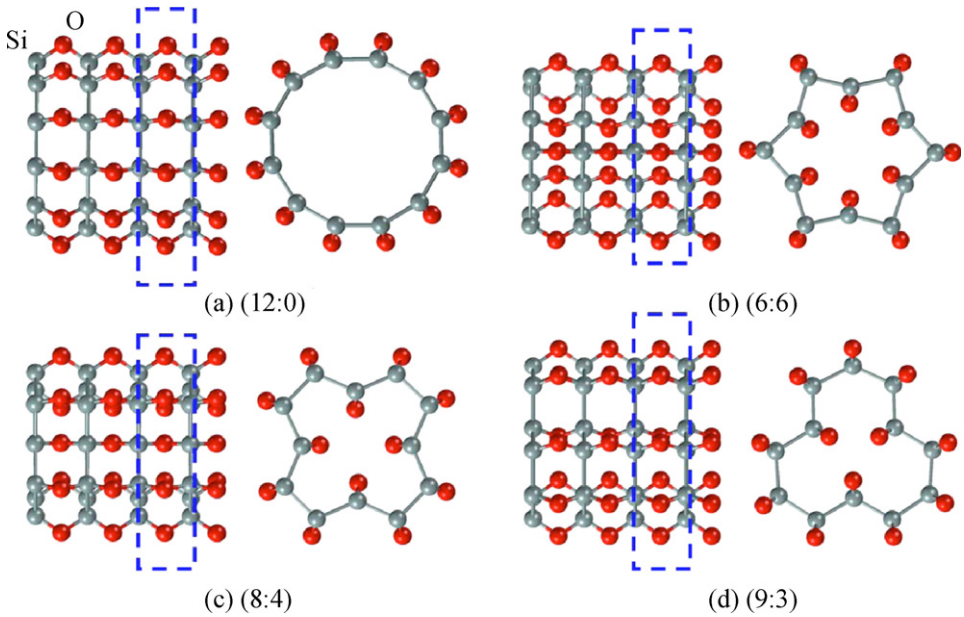

Fig. 12. The representative isomers of the SiO nanotubes built by stacking silicon dodecagons via Si–O–Si binding. Here (n_1:n_2) denotes the numbers of the exterior and the interior oxygen atoms per supercell, respectively. The rectangles with dashed lines represent the sizes of the supercells. (Reprinted with permission from Ref. [72]. Copyright 2007 American Institute of Physics.)

are narrow-band-gap semiconductors with the band-gap varying from 0.17 to 0.84 eV. The band-gap is sensitive to the surface structure of the nanotubes.

Recently, Palaria et al. [73] developed a general procedure for the prediction of the atomic structure of nanoscale materials and applied it to SiNTs. They found various low-energy structures with similar stability (within 0.07 eV/atom of one another) but with widely different atomic structures and disparate elastic properties (Young's moduli within a factor of ca. 3). These SiNT structures exhibit low symmetry and bonding environments significantly different from those known for bulk silicon.

4.2.2. *Double-walled sp^3 SiNTs*

The structures of a number of theoretically proposed double-walled silicon nanotubes (DWSiNTs) with faceted wall surfaces have been calculated from first-principle calculations [65]. As mentioned above, cylindrical DWSiNTs (such as (9,0)@(15,0) depicted in Fig. 13(c)) are quite unstable at room temperature. They easily distort and transform into amorphous SiNTs by the formation of additional covalent bonds between the inner and the outer walls. However, by carefully controlling the annealing process in the molecular dynamic calculations, a DWSiNT can be obtained. The resulting "transformed" double-walled silicon nanotube has a hexagonal shape and is dubbed *h*-DWSiNT; one example, *h*-(9,0)@(15,0) is shown in Fig. 13(d). It has the lowest E_{form} than any of its amorphous isomers. The nearest Si–Si distance between the inner and the outer walls of *h*-DWSiNT is 2.41 Å, indicating the formation of single Si–Si covalent bonds. Half of the silicon atoms in this *h*-DWSiNT are fourfold coordinated as compared to the purely threefold coordinated cylindrical SWSiNT. Multi-walled SiNTs with larger diameters and wall thicknesses can likewise be built. Another form of DWSiNT, dubbed tetrahedral *t*-DWSiNT was also considered in Zhao et al.'s work. They can be built by the following steps. The initial configuration of the *h*-DWSiNT with hexagonal cross-section enclosed by four {1 1 1} faceted surfaces and two {0 0 1} facets and tube axis oriented along the <1 1 0> direction was created by cutting from bulk silicon. This hexagonal prism was then heated at 500 K for 2 ps and subsequently cooled down to 0.1 K for 1.0 ps to obtain the equilibrium configuration (as shown in Fig. 13(e)). (2×1) dimerization along the axial direction occurred on the two reconstructed {0 0 1} surfaces, whereas the four {1 1 1} facets undergo considerable distortion. However, the tetrahedral feature of the atomic arrangement is maintained in this highly deformed *t*-DWSiNT. The highly symmetric *h*-DWSiNT and the deformed *t*-DWSiNT have very close formation energies with a difference of <0.2 meV/atom; both were claimed to be energetically more favorable (by 0.078 eV/atom) than the silicon nanowire of 1.15 nm in diameter (Fig. 13(f)), but their electronic structures are quite different. The pristine *h*-DWSiNT has an indirect band-gap of 0.21 eV (see Fig. 14(a)), which is much narrower than that of bulk silicon. However, the *t*-DWSiNT has a direct band-gap of 0.11 eV at Γ point (see Fig. 14(b)). The corresponding hydrogen-passivated *h*-DWSiNT and the deformed *t*-DWSiNT were also considered. As can be seen from Fig. 14(c) and (d), the band-gaps widen to 1.32 and 1.55 eV for the *h*-DWSiNT and the *t*-DWSiNT, respectively. The hydrogen-passivated *h*-DWSiNT has an indirect band-gap with the top of HOVB and the bottom of LUCB at Γ and (0,0,3/4) π/a points, respectively, whereas the hydrogen passivated *t*-DWSiNT has a direct band-gap at Γ point.

4.3. *Crystalline silicon nanotubes (cSiNTs)*

Though attempts to make *bona fide* CNT-like SiNTs, have thus far been unsuccessful, the closely related tube-like silicon nanostructure, known as crystalline silicon nanotubes (cSiNTs) had been synthesized by several groups. This silicon nanostructure, however, is best described as rigid crystalline silicon pipes or hollow crystalline silicon nanorods [51–55].

4.3.1. *Preparation of cSiNTs via various templates*

Beside being an interesting nanostructure, crystalline silicon nanotubes may open up new and exciting possibilities for making different kinds of nanosized heterostructures by filling the inside (hollow) space with one type of nanomaterial and/or by decorating the outside surfaces of the nanotubes with yet another type of nanomaterial to produce integrated nanodevices. Such possibilities have been well demonstrated for CNTs.

We shall describe several synthetic routes to cSiNTs.

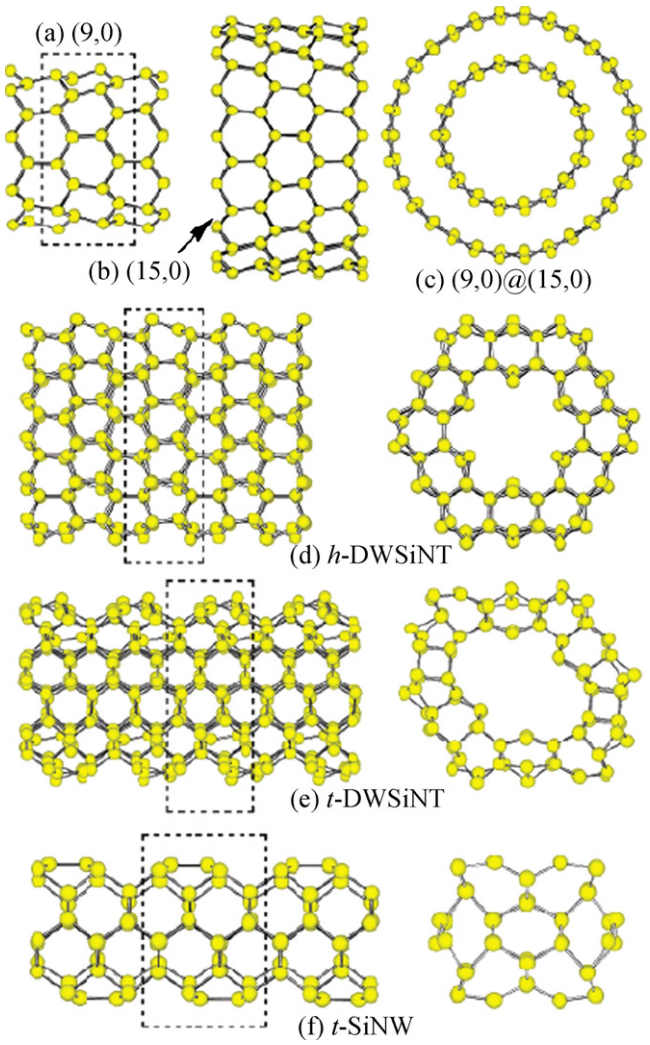

Fig. 13. Equilibrium configurations of SiNTs and a SiNW. Side view of (a) (9,0) and (b) (15,0) gear-like *g*-SWSiNTs; (c) top view of a cylindrical DWSiNT built by assembling (9,0) and (15,0) *g*-SWSiNTs with a coaxial structure; side view (left) and top view (right) of (d) *h*-DWSiNT, (e) *t*-DWSiNT, and (f) *t*-SiNW. (Reprinted with permission from Ref. [65]. Copyright 2007 American Chemical Society.)

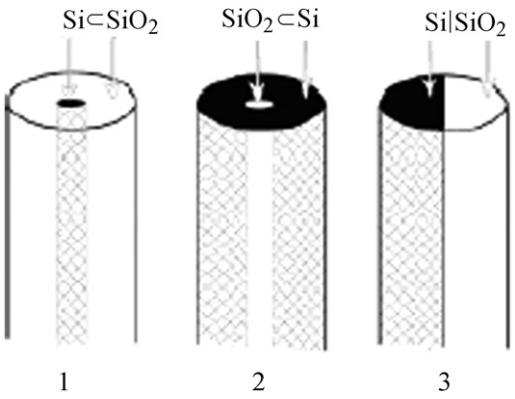

Scheme 1. Three distinct types of composite nanowires and nanotubes of silicon and silica.

4.3.1.1. Using zeolites as templates. In one example, cSiNTs was prepared unexpectedly when zeolites were used as a sacrificial template to grow very fine and uniform silicon nanostructures [55,74]. In fact, three distinct types of composite nanowires and nanotubes of (crystalline) silicon and (amorphous) silica were grown simultaneously on zeolite Y via disproportionation of SiO by thermal evaporation: namely, a silicon nanowire *inside* a silica nanotube (**1**); a silicon nanotube *outside* a silica nanowire (**2**); and a *side-by-side* growth of a biaxial silicon–silica nanowire structure (**3**), as shown schematically in Scheme 1 [55]. The second type, $SiO_2NW \subset cSiNT$, can be described as a crystalline silicon nanotube filled with amorphous silica (or a silicon nanotube *outside* a silica nanowire). (Here radial heterostructures are designated as $A \subset B$ where A and B are nanowires and nanotubes, respectively.)

TEM images of a representative $SiO_2NW \subset cSiNT$ are shown in Fig. 15. It has an inner diameter of 3 nm and an outer diameter of 15 nm. The crystalline silicon walls have a thickness of about 6 nm on each side. The crystal lattices on the two sides of the tube are almost parallel (within 10° in most cases). The distinctive features of these cSiNTs are: (1) single-crystalline tube walls; (2) uniform inner and outer tube diameters throughout the length of the wire; and (3) the tube interior are filled with silica. Besides, this method is rather simple and requires no catalysts.

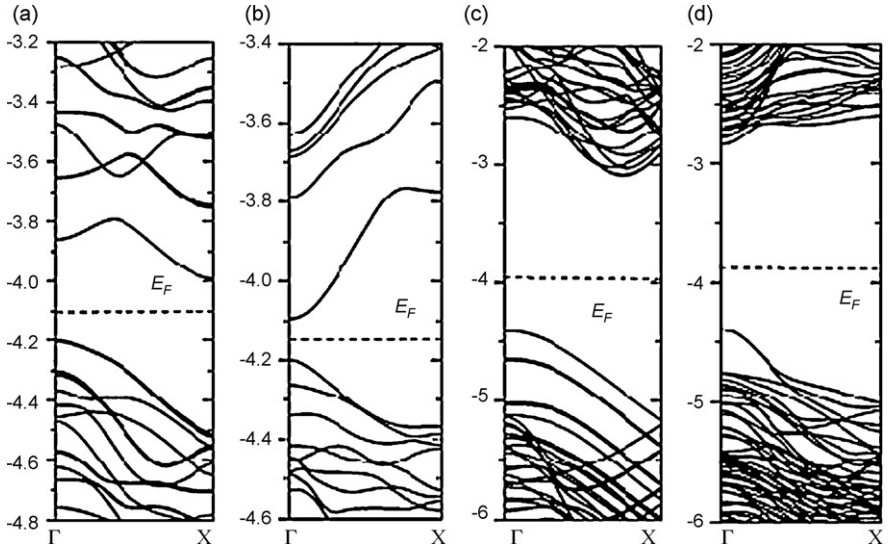

Fig. 14. Band structures of pristine (a) *h*-DWSiNT and (b) *t*-DWSiNT and hydrogen-passivated (c) *h*-DWSiNT and (d) *t*-DWSiNT along (0,0,0) π/a–X (0,0,1) π/a direction. The dashed lines indicate the Fermi level. (Reprinted with permission from Ref. [65]. Copyright 2007 American Chemical Society.)

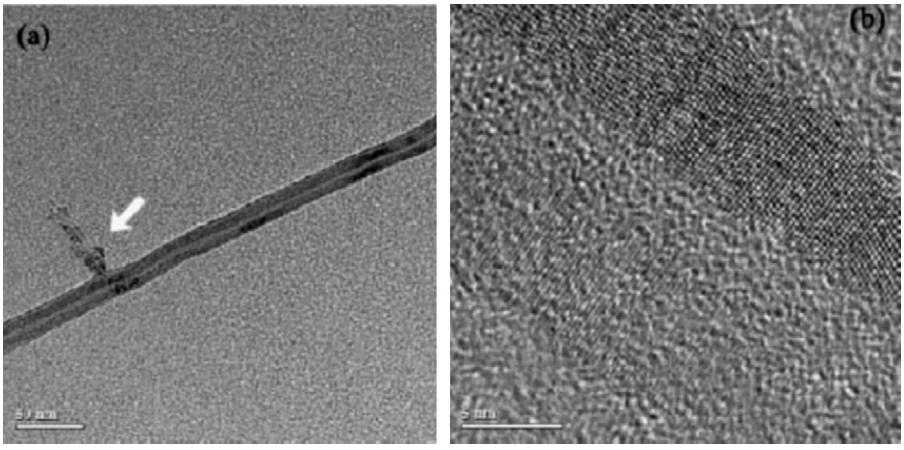

Fig. 15. (a) TEM of a crystalline silicon nanotube. (b) Corresponding HRTEM image. (Reprinted with permission from Ref. [55]. Copyright 2003 American Chemical Society.)

4.3.1.2. Using AAO as templates. Independent works by several other groups to produce cSiNTs are worth mentioning. For example, Sha et al. [51] produced a somewhat different cSiNT structure with the tube wall being made of polycrystalline (pc) silicon interlaced with amorphous silicon. These pcSiNTs were prepared by chemical vapor deposition (CVD) using a nanochannel Al_2O_3 substrate (i.e., the AAO membrane) as template. In this case, the channels were pre-sputtered with gold which served as a catalyst for the VLS growth of the pcSiNTs (along with SiNWs) inside the AAO nanochannels. Jeong et al. [52] also reported the growth of polycrystalline or amorphous SiNTs, with thick SiO_2 sheaths, by molecular beam epitaxy on top of the protruding pore edges of the AAO membrane, but without metal catalysts.

4.3.1.3. "Template replication" technique. Another interesting strategy to produce cSiNT using AAO is the so-called "template replication" method from which highly ordered pcSiNT arrays can be prepared [53]. The method involves a combination of a multi-step template replication (with NiO cores inside AAO nanochannels) technique and the CVD (using silane) approach. By dissolving away the NiO cores and the AAO templates, pcSiNTs of uniform diameters, lengths, and wall thickness can be obtained (see Fig. 16).

4.3.1.4. Using ZnS nanowires as templates. Recently, Hu et al. [54] demonstrated an epitaxial casting technique in producing cSiNTs using ZnS nanowires as templates. In the template-based growth of the crystalline Si tubular nanostructures, ZnSNW ⊂ cSiNT core–shell nanowires were initially obtained by epitaxial growth of Si shell layer on ZnS nanowires as templates, in which the shell is a Si thin layer, and the core is a ZnS nanowire. The ZnS nanowire templates were subsequently removed from the ZnSNW ⊂ cSiNT core–shell nanowires with HCl solution which resulted in the formation of the crystalline Si tubular nanostructures, cSiNTs. Some nanotubes have one closed end (Fig. 17(a)), while others are open-ended (Fig. 17(c)). The high-resolution TEM image of a crystalline tubular nanostructure shows that the (1 1 1) fringes with a d spacing of about 0.31 nm are aligned perpendicular to the longitudinal direction of the tube, suggesting a <1 1 1> growth orientation of the single-crystalline Si tubular domains.

4.3.2. Theoretical investigations of crystalline silicon nanotubes

A recent report by Yan et al. investigated the structures and properties of single-crystalline SiNTs using the first-principle method [75]. These SiNTs, constructed by the bulk-like tetrahedrally coordinated Si atoms with sp^3 hybridization, were energetically stable. Its electronic property is sensitive to the external diameter, tube-wall thickness, and tube-axis orientation due to quantum confinement effects. A direct band-gap is observed in SiNTs with smaller sizes. The band-gap increases monotonically with decreasing tube-wall thickness, in accord with the substantial blue shift observed in the experiment. In a later study [76], the quantum confinement behavior, electronic, and optical properties of cSiNTs with non-uniform wall thickness were further investigated through first-principle calculations. The distributions of wave functions of the VBM, CBM, and PDOS imply that the carriers (electrons and holes) may be mainly confined on the thicker sides. The band-gap decreases and the absorption spectra show a red shift with the enlargement of the "effective confinement region". Based on the effects of non-uniform wall thickness on wave functions of the VBM and CBM of the SiNT, a new modulation doping method, i.e., the selective *p*-/*n*-type doping on the thinner side, was proposed to improve the carrier mobility and transconductance of doped cSiNTs with non-uniform wall thickness.

5. SiC nanowires (SiCNWs)

Among the various semiconducting materials, silicon carbide possesses unique physical and electronic properties which make it a suitable material for the fabrication of electronic devices for high temperature, high power, and high frequency applications [77]. One-dimensional SiC nanosystems may exhibit unique properties due to quantum-size effects, making them useful materials in nanotechnology and nanoscale engineering [78]. Silicon carbide nanomaterials have a great potential for application in chemical sensors in harsh environment or in biological sensors. It is of interest to explore their structural and electronic properties.

We shall discuss silicon carbide nanowires (SiCNWs) in this section. Experimentally, there are many ways to synthesize SiCNWs [79,80]. However, there are relatively few theoretical reports [81].

Silicon carbide (SiC) is a covalent material with many polytypes. The cubic phase, which has essentially zero formation energy, dominates in SiCNWs. Experimentally, well-separated and equal-spaced twins had been observed in SiCNWs. Shim et al. [82] presented a model to account for the twinning. This model is based on the energy minimization of interfaces and edges near twin boundaries. Their theoretical result shows that the distance between neighboring twin boundaries is equal to 18–31% of the diameter for SiCNWs, consistent with the experimental observation.

The thermal conductivity of SiCNWs is significantly reduced in comparison with the bulk phase. Generally it also depends on the presence of defects on the surface, shown by non-equilibrium classical MD simulations [83]. First-principle calculations [84]

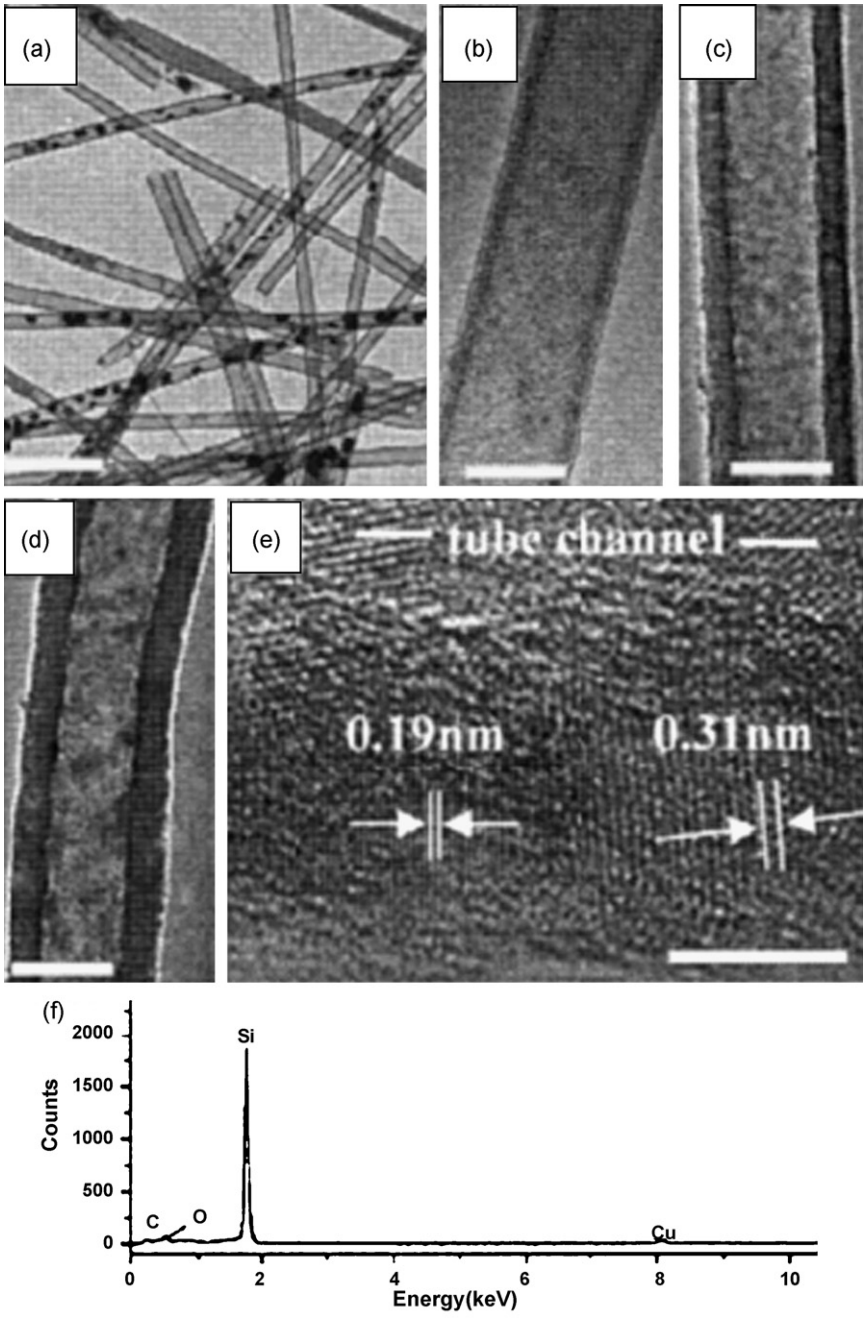

Fig. 16. TEM image of (a) the pcSiNTs, and (b)–(d) the individual pcSiNT with different wall thicknesses. Scale bar: (a) 250 nm and (b)–(d) 50 nm. (e) High-resolution TEM image of the SiNT. Scale bar: 5 nm. (f) EDS spectrum taken from an individual SiNT. (Reprinted with permission from Ref. [53]. Copyright 2005 American Institute of Physics.)

of the mechanical properties, electronic structure, and uniaxial-stress effects of β-SiCNWs have found that the band-gap of SiCNWs becomes larger as their diameter decreases because of the quantum confinement effect, but increases (decreases) slightly with increasing tensile (compressive) stress up to about 12 GPa. The calculated Young's modulus and tensile strength of SiCNWs are about 620 and 52 GPa, respectively, in accordance with the experimental data. The characteristics of their mechanical and electronic properties suggest that β-SiCNWs may be used in electronic composites as reinforcement nanomaterials or in nanoscale electronic/photoelectric devices under harsh environments.

Makeev et al. have investigated the elastic properties of 3C-SiCNWs of different diameters and structural changes, upon application of external loadings, using GTBMD simulations [85]. It was shown that, under axial compression and tensile strain, the computed Young's modulus and structural changes at elastic limit do not depend appreciably on the diameter of the nanowire except for the nanowire of the smallest diameter (≈1 nm) under compression. The elastic modulus and structural failure near the elastic limit regime, for nonaxial bending and torsional strains, depend strongly on the nanowire diameters through a power-law behavior.

Wang et al. extended the study of the nanomechanical behavior of <1 1 1>-oriented β-SiCNWs under tension, compression, torsion, combined tension–torsion, and combined compression–torsion by GTBMD simulations [86]. Under axial tensile strain, the bonds of the NWs are just stretched before the failure of NWs by bond breakage. The failure behavior depended on size and temperature. Under

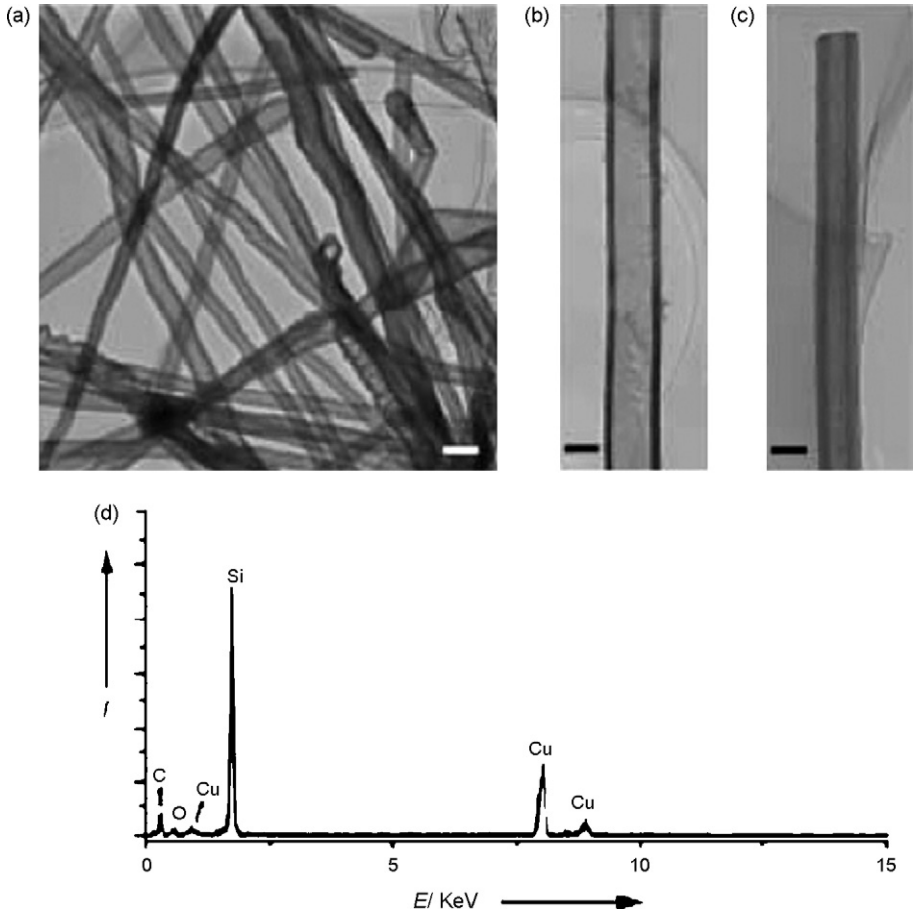

Fig. 17. (a) TEM image of cSiNTs. Scale bar: 200 nm. (b) TEM image displaying a Si nanotube with a thin wall. (c) TEM image displaying the open end of a Si nanotube. Scale bars in (b) and (c): 100 nm. (d) EDS spectrum taken from an individual Si tubular nanostructure. (Reprinted with permission from Ref. [54]. Copyright 2004 Wiley–VCH.)

axial compressive strain, the collapse of the SiCNWs by yielding or column buckling mode depends on the length and diameters of the NWs, and the latter is consistent with the analysis of equivalent continuum structures using Euler buckling theory. The NWs collapse through a phase transformation – from crystal to amorphous structure – in several atomic layers under torsion strain.

The size-dependence of surface stress, surface stiffness, and Young's modulus of hexagonal prism <1 1 1>-oriented β-SiC nanowires have been reported [87]. The edge and surface effects become more significant as the cross-sectional area of a nanowire becomes smaller.

6. Silicon carbide nanotubes (SiCNTs)

6.1. Synthesis of SiCNWs, biaxial SiC|SiO_2 NWs, and SiCNTs using CNTs as reactive templates

Despite the unsuccessful attempts to make *bona fide* SiNTs by many research groups, CNT-like silicon carbide nanotubes (SiCNTs) have recently been successfully synthesized and characterized. In this subsection, we shall describe the synthesis of SiCNT using CNT as a reactive template, thereby producing a new composite heterostructure of CNT ⊂ SiCNT [21].

The growth of one-dimensional nanostructures of SiC was first observed in the reaction between silicon (produced by disproportionation of SiO) and carbon nanotubes (as templates) in a tube furnace (at about 935 °C). The original goal of this particular experimental work was to synthesize SiNTs (see Section 3) using CNTs as templates. Instead, three types of interesting SiC nanostructures were obtained. The first type is the silicon carbide nanowires with 2.5 Å spacing of the {1 1 1} planes of β-SiC with the cubic zinc blende structure. These nanomaterials are similar to those produced by Pan et al. [88]. The second nanostructure obtained was the biaxial nanowires of silicon carbide-silicon oxide (see Fig. 3(a) and (b) of Ref. [89]). A similar biaxial structure had been observed by Wang et al. [89].

A third type of nanostructure may be described as CNT ⊂ SiCNT. A typical image is shown in Fig. 18(a). Element mappings (Figs. 18(b) and (c)) showed the multi-walled tube structures to be composed of Si and C with the interior being CNTs and the exterior being SiCNTs. Furthermore, the interlayer spacings of the exterior multi-walled SiCNTs are significantly larger than 3.4 Å observed for the interior multi-walled CNTs (see Fig. 18(a)) [21].

It is known that at a sufficiently high temperature ($T > 800$ °C), Si can react with C to form silicon carbide [90]. At the experimental temperature of 935 °C described above Si and C react to form SiC. The transformation of carbon nanotube to a silicon carbide nanotube is controlled by the diffusion of Si to the SiC/C interface. However, since the Si diffusion rate through bulk SiC is extremely slow in the temperature range of 800–1000 °C, a steady supply of Si atoms from the disproportionation of SiO must therefore be transported primarily via surface diffusion [91]. This is consistent with the observation that the SiCNTs were formed layer by layer, from outside in, via diffusion of Si atoms into the multi-walled carbon nanotube [21].

The EELS spectrum (curve (a) in Fig. 19) of a single multi-walled SiCNT shows that the Si $L_{3,2}$-edge shifts to a higher energy at 101.2 eV (from 99.3 eV of pure silicon) and the C K-edge shifts to

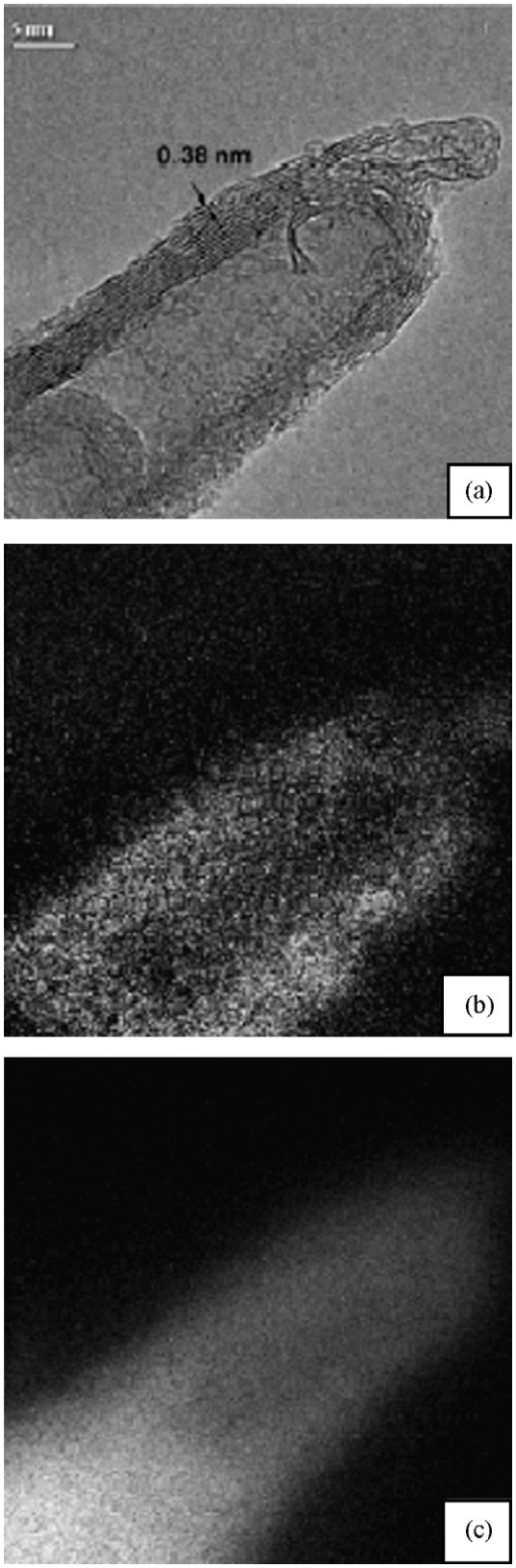

Fig. 18. (a) HRTEM image of a SiC nanotube structure with 3.8 Å interlayer spacing. Panels (b) and (c) are Si and C element mappings of the SiC nanotube in (a), respectively. (Reprinted with permission from Ref. [21]. Copyright 2002 American Chemical Society.)

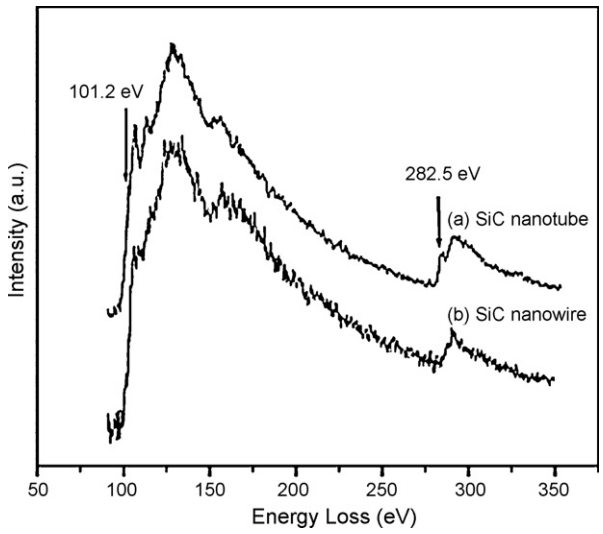

Fig. 19. EELS spectra of (a) a single SiC nanotube and (b) a single SiC nanowire. (Reprinted with permission from Ref. [21]. Copyright 2002 American Chemical Society.)

a low energy at 282.5 eV (from 284 eV of pure carbon), indicating a strong chemical bonding between Si and C. This is to be expected based on the fact that carbon is more electronegative than silicon. The EELS of SiCNT is contrasted with the EELS of β-SiC nanowire (curve (b) in Fig. 19). With the exception of the pre-edge peaks, the two EELS spectra are rather similar. The strong pre-edge absorption peaks of both the silicon and the carbon EELS of SiCNT (curve (a) of Fig. 19) are indicative of the π bonding between Si and C (compare with curve (b) of Fig. 19 for β-SiC).

The observed multi-walled SiC nanotube is a new polytype (allotrope) of SiC, with interlayer spacings, ranging from 3.5 to 4.5 Å, distinctly different from those of the amorphous SiC or any of the common crystalline SiC phases (such as the cubic (3C or β), hexagonal (4H, 6H), or rhombohedral (15R) structures, etc.) [87]. It was also proposed that the structure of these new SiC nanotubes is similar to that of carbon nanotubes with silicon atoms replacing half of the carbon atoms.

6.2. Theoretical studies of SiCNT structures

6.2.1. Single-walled sp^2 SiCNTs

Here we discuss briefly two theoretical studies of SiCNTs. In one study, *ab initio* methods were used by Froudakis and coworkers [92] to study SiCNTs with different Si:C ratios, ranging from C-rich to Si-rich (Fig. 20). SiCNTs gradually lose stability as the Si:C ratio increases. Nevertheless they remain stable until the ratio of 1:1; after which the Si-rich tubes collapse to nanowires or clusters with solid interiors. In another study [93], the generalized tight-binding molecular dynamics (GTBMD) scheme of Menon and Subbaswamy and *ab initio* methods were used to investigate the structural and electronic properties of SiCNTs with Si:C ratio of 1:1. Two types of rolled-up-graphene-sheet structures of SiCNTs were studied: type 1 involves alternate Si and C sites (Fig. 21) whereas type 2 contains pairs of Si=Si and C=C bonds (Fig. 22). Surface reconstruction, after relaxation, results in wave-like appearance for both structures, with the Si atoms situated in one plane and the C atoms located above and below the Si plane. However, the wave-like distortion is more severe for type 1 structures. The SiCNTs with alternating Si–C bonds are energetically preferred over the forms which contain C–C or Si–Si bonds. Classical MD simulations [94] show that SWSiCNTs are more stable than nanowires below a critical diameter of about 1.6 nm, while

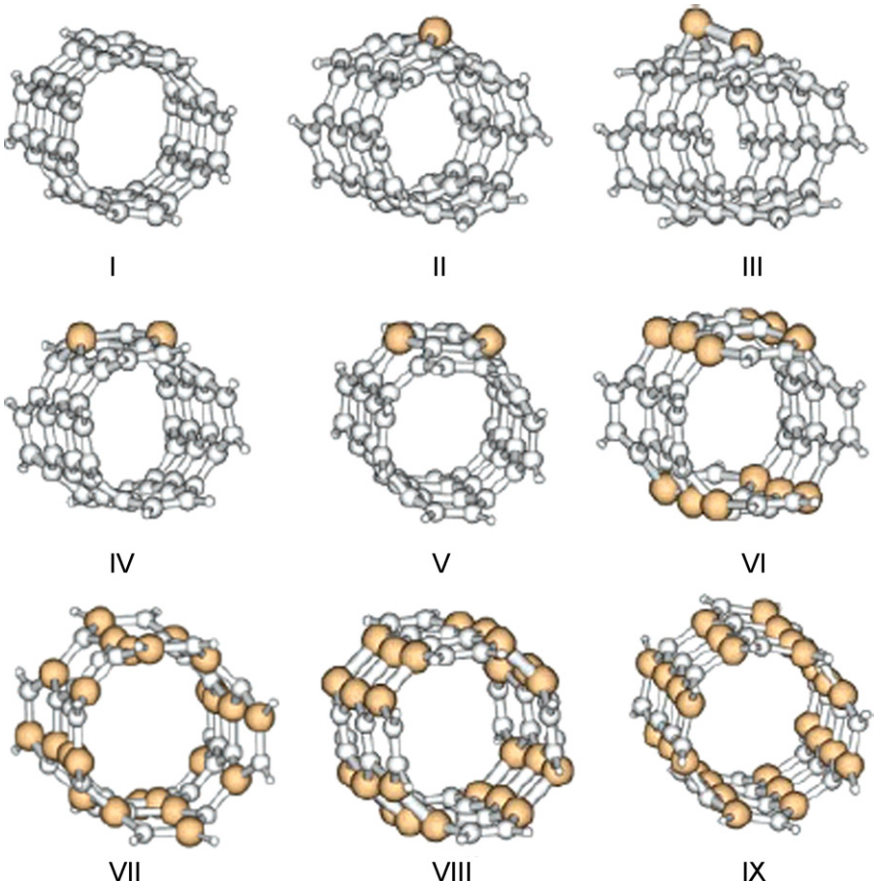

Fig. 20. DFT optimized geometries of finite-sized, single-walled silicon-carbon nanotubes (SiCNT) with various Si/C ratios. (Reprinted with permission from Ref. [92]. Copyright 2003 American Chemical Society.)

SiC nanowires (SiCNW) are more stable than nanotubes beyond that.

The dependence of the electronic and optical properties of single-walled zigzag (n,0), armchair (n,n), and chiral (n,m) SiCNTs on the tube diameter has been investigated by DFT [95,96]. It was shown that the zigzag SiCNTs are direct-gap semiconductors, while the armchair and chiral tubes are indirect-gap semiconductors. The band-gap increases with increasing tube diameter. This has been attributed to smaller π–σ hybridizations and larger repulsions between π and π* states as the diameter increases. For all SiCNTs, the top of the valence-band region mainly arises from C-2p states with a small mixing of Si-3s,3p states, and the conduction bands above the Fermi level are mainly due to Si-3p states.

The zero frequency dielectric constants $\varepsilon_x(0)$ and $\varepsilon_z(0)$ decrease monotonically as the diameter of SiCNTs increases. The same phenomenon happens in single-walled BN nanotubes [97]. For a given SiC nanotube, $\varepsilon_z(0)$ is larger than $\varepsilon_x(0)$, i.e., the zero frequency dielectric constant along the tube axis is larger than that

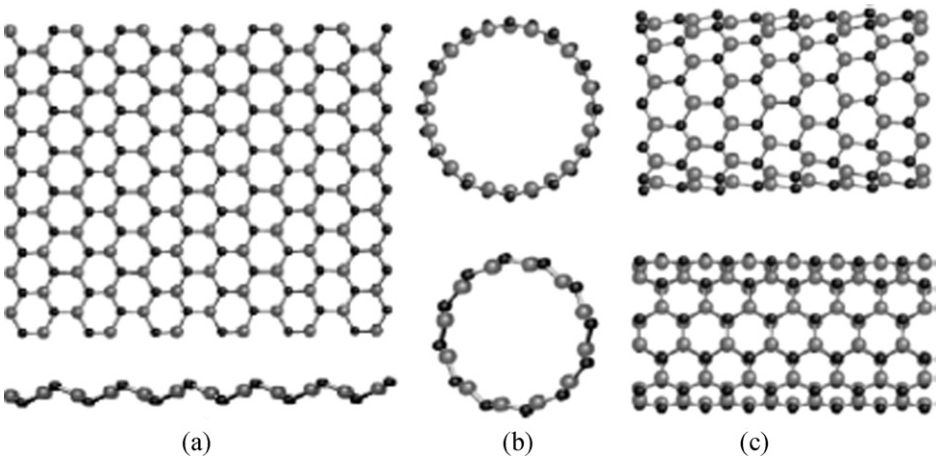

Fig. 21. (a) Type-1 graphene sheets of SiC with a Si to C ratio of 1:1 obtained by GTBMD relaxation. The surface reconstruction results in wave-like appearance. The top and bottom panels in each of these figures show top and side views of the structures, respectively. In both structures Si atoms (colored gray) are all in a single plane, while C atoms (colored black) are displaced above and below this plane. (b) End views of single-wall SiC nanotubes of zigzag (top panel) and armchair (bottom panel) configurations. (c) Corresponding side views. (Reprinted with permission from Ref. [93] (http://link.aps.org/abstract/PRB/v69/p115322). Copyright 2004 by the American Physical Society.)

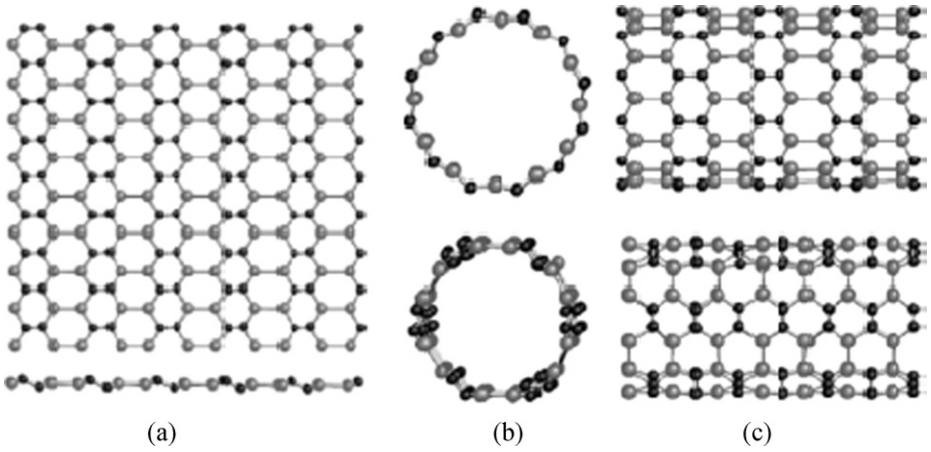

Fig. 22. (a) Type-2 graphene sheets of SiC with a Si to C ratio of 1:1 obtained by GTBMD relaxation. (See caption for Fig. 21a for color designations.) (b) End views of single-wall SiC nanotubes of zigzag (top panel) and armchair (bottom panel) configurations. (c) Corresponding side views. (Reprinted with permission from Ref. [93] (http://link.aps.org/abstract/PRB/v69/p115322). Copyright 2004 by the American Physical Society.)

perpendicular to the tube axis, owing to the quantum confinement effect in the perpendicular direction. Fig. 23 shows the imaginary parts of the dielectric functions of armchair and zigzag SiCNTs when the electric field of the electromagnetic wave is parallel to the tube axis. For both armchair and zigzag SiCNTs, the spectra can be divided into two regions, namely, the low-energy range from 0 to 5 eV and the high-energy range from 5 to 20 eV. The peak at the low-energy region is stronger than the one at the high-energy region. The first peak is mainly due to the electronic transitions from C-2*p* bonding orbitals to Si-3*p* nonbonding orbitals (inter-π band transition). This peak is slightly blue shifted with increasing tube diameter. The second peak originates from the Si–C π band to π^* band transition.

The DFT studies [98] of the electronic properties of SiCNTs of different tube lengths have shown that increasing the nanotube length yields a higher localization of the lowest unoccupied and highest occupied molecular orbitals (LUMO and HOMO), thus affecting the behavior of the band-gap and chemical reactivity of the SiCNTs. The structural stability also increases with increasing tube length and diameter.

Like CNTs and cSiNTs, silicon carbide nanotubes can also be made into various nanostructures by filling the inside (hollow) space or by decorating the outside surfaces with nanomaterials. In one study, the structures and optical properties of single-wall SiC nanotubes filled with metal halides MCl (M = K, Ag) have been investigated via first-principle calculations [99]. The M–Cl distances perpendicular to the tube axis are slightly smaller than the ones parallel to the tube axis, which can be attributed to the interactions between MCl and the tube wall. AgCl affects the structures and properties of SiC nanotubes more significantly than KCl, and that the interaction between the nanotube and the encapsulated halide is stronger for narrower SiC nanotube. The AgCl incorporation into SiCNTs also results in band-gap narrowing. In another study, using hybrid DFT (HDFT) and a finite cluster approximation, it was demonstrated that the properties of zigzag SiC nanotubes can be modified by filling the inside, or by decorating the outside (adsorption) of SiCNTs with iron atoms [100]. The structures studied have magnetic ground states with high magnetic moments, suggesting the possibility of using these nanomaterials in spintronics applications.

The electronic and atomic structures of SiCNTs can be modified by sidewall decoration, such as H, XH_3 radical X = {C, Si}, N and NH_x (x = 1, 2) [101–103]. The *exo*-hydrogenation of a single C atom results in acceptor states close to the highest occupied valence band of pristine SiCNT, whereas donor states close to the lowest unoccupied conduction band appear as a Si atom being hydrogenated, as shown in Fig. 24. Upon fully hydrogenating the Si atoms, (8,0) and (6,6) SiCNTs become metallic with very high density of states at the Fermi level. The full hydrogenation of C atoms, on the other hand, increases the band-gap to 2.6 eV for (8,0) SiCNT and decreases the band-gap to 1.47 eV for (6,6) SiCNT, respectively. The band-gap of SiCNTs can also be greatly increased through the hydrogenation of all the atoms. The XH_3 radicals can be chemically adsorbed onto

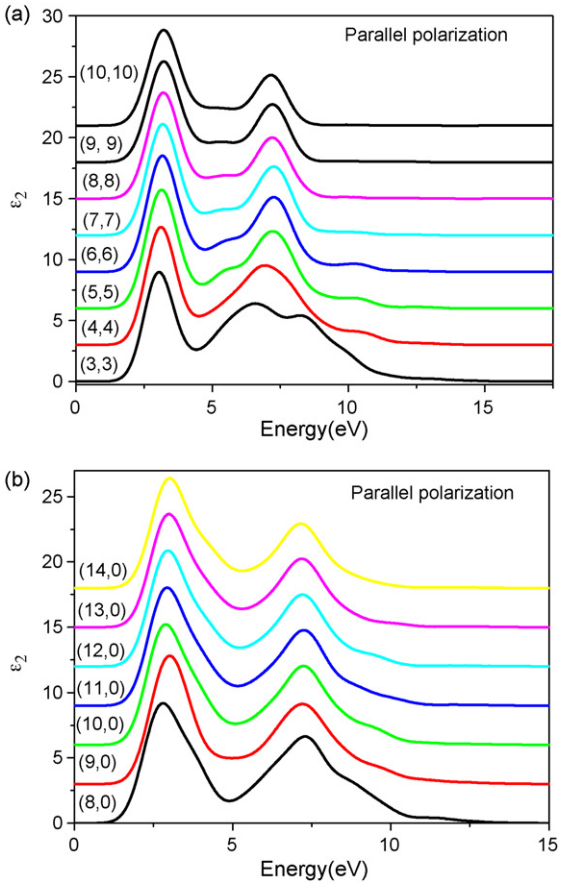

Fig. 23. The imaginary parts of the dielectric functions under parallel polarization: (a) armchair SiCNTs and (b) zigzag SiCNTs. (Reprinted with permission from Ref. [95]. Copyright 2007 The Optical Society of America.)

Si sites or C sites on the tube wall, with the adsorption energies ranging from −2.01 to −2.90 eV for a (5,5) SiCNT. The modification of the electronic structures of these decorated SiCNTs depends mainly on the adsorption site rather than the XH_3 species. The electronic structures of XH_3-decorated SiCNTs exhibit characteristics of *n*-type semiconductors for XH_3 adsorbed on a C atom, whereas *p*-type semiconductors can be achieved by XH_3 adsorption on a Si atom. The N and NH_x ($x = 1, 2$) groups can be chemically incorporated into the network of SiCNTs in different ways, accompanied by the formation of N–C and N–Si bonds. It is apparent that the electronic structures of SiCNTs can be effectively modified by these groups and display diverse characters ranging from semiconducting to semimetallic, depending on the chirality of SiCNTs nature of the functional group, and the incorporation site. These results are expected to open ways to tune the electronic structures of SiCNTs which may have promising applications in building nanodevices.

SiCNTs can also be functionalized by transition metal atoms. Zhao and Ding [104] reported DFT studies of the adsorption of a series of TM atoms on SWSiCNTs. The physical properties of the SWSiCNTs are altered significantly by metal functionalization. Moreover, the modifications in the electronic structures of most of the metal-functionalized SWSiCNTs are little influenced by the location of the adsorption site. An exception is Ti, in which the electronic properties can vary with the adsorption site. Interestingly, the (8,0) single-walled SiC nanotube exhibits metallic characteristics when Ti adsorbs on hexagonal sites and characteristics of a smaller-band-gap semiconductor when Ti adsorbs on carbon sites. The results suggest that transition metal-SiC nanotube materials could be used in interesting applications in the fabrication of gas-sensor devices, catalysts, or one-dimensional nanoconductors or nanomagnets, among others.

Spin-polarized DFT (SP-DFT) was used to investigate the electronic and structural properties of vacancies and "antisites" in zigzag, armchair, and chiral SiCNTs [105]. Antisites present lower formation energies (compared to vacancies), and introduce an empty electronic level close to the bottom of the conduction band for both cases Si_C and C_{Si}. A carbon vacancy introduces a pair of electronic levels (bonding and antibonding) within the band-gap. A silicon vacancy presents the highest formation energy and introduces one occupied level (spin up) resonant within the valence band and three nearly degenerate spin-polarized levels, one for spin up and two for spin down, within the nanotube band-gap.

N and B atoms are common contaminants in bulk SiC. Nitrogen preferentially substitutes the C site, making *n*-type conductivity in bulk SiC. B substitutes both C and Si sites, forming a deep and a shallow acceptor in bulk SiC, respectively. Gali [106] studied the effects of these substitutions for armchair and zigzag SiCNTs by *ab initio* supercell calculations. Nitrogen forms relatively shallow or deep donor state depending on the width of the band-gap of the SiCNT. There is a significant difference in the band structures of N-substituted armchair vs. zigzag SiCNTs. In contrast, boron is a relatively deep or shallow acceptor at C and Si sites, respectively, like in bulk SiC polytypes. The site preference of boron depends on

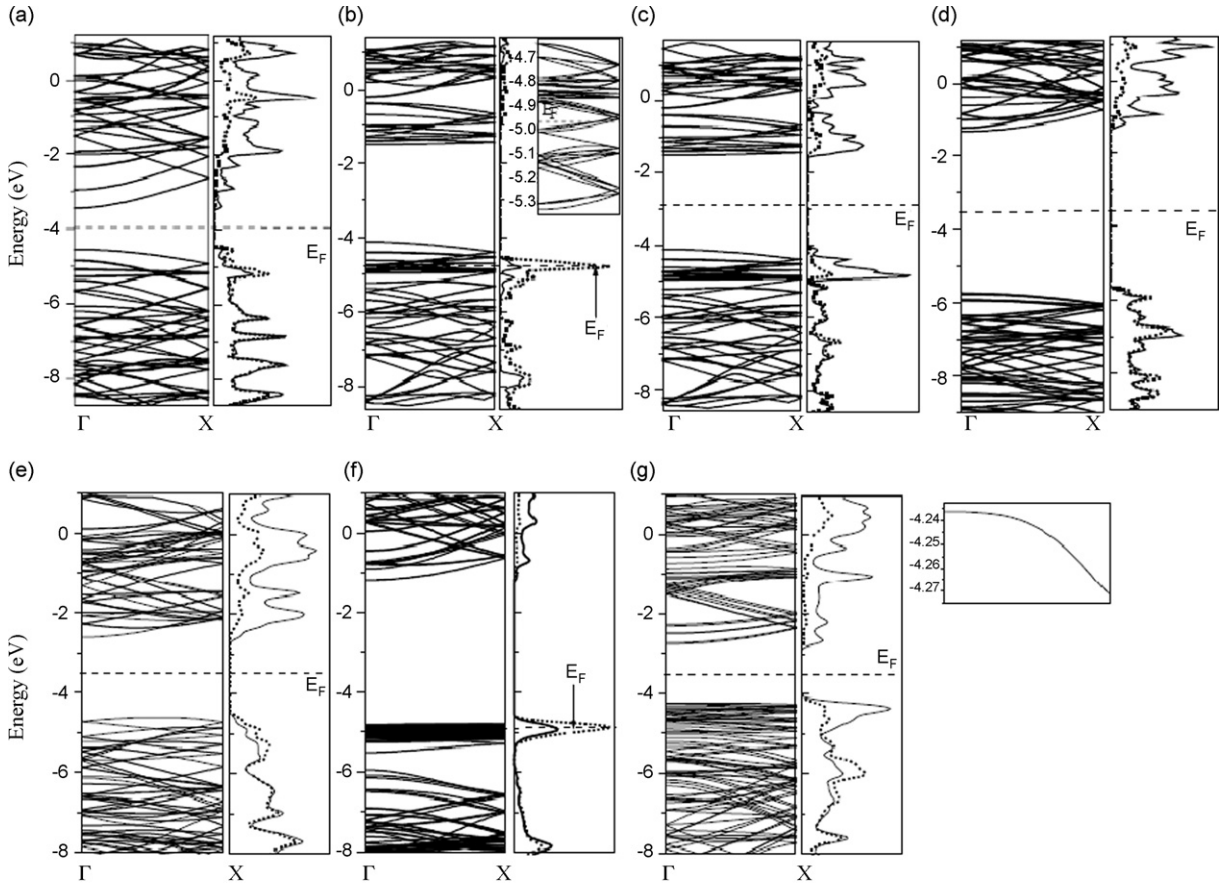

Fig. 24. The band structures and density of states of (a) pristine (8,0) SiCNT; (b) (8,0) SiCNT with each Si atom being hydrogenated; (c) (8,0) SiCNT with each C atom being hydrogenated; (d) (8,0) SiCNT with each atom being hydrogenated; (e) pristine (6,6) SiCNT; (f) (6,6) SiCNT with each Si atom being hydrogenated; (g) (6,6) SiCNT with each C atom being hydrogenated (the HOVB of this tube is shown as the inset of this figure). The density of states are projected onto Si (represented by the solid lines) and C atom (the dotted lines), separately. The dash lines denote the Fermi levels (E_F). (Reprinted with permission from Ref. [101]. Copyright 2005 American Institute of Physics.)

the stoichiometry of the SiCNTs. There is no significant difference in the properties of B-substituted SiCNTs between armchair and zigzag NTs.

6.2.2. Bundled sp^2 SiCNTs

The DFT studies of the structural and electronic properties of bundled (8,0) and (6,6) SiCNTs have shown that for such small-diameter nanotubes the inter-tube interaction causes a very small radial deformation, while band splitting and reduction of the semiconducting energy band-gap are significant [107]. There is a larger inter-tube separation and weaker inter-tube interaction in the (8,0) SiCNT bundle with respect to (10,0) CNT bundle, although they have the same radius. Almost at the same time, Moradian et al. [108] reported results of *ab initio* DFT calculations of the structural and electronic properties of bundles of large-diameter armchair (13,13) and (14,14) SiCNTs. They found that the cross-sections of these large-diameter SiCNTs in the bundle have rounded hexagonal shape. As expected, the inter-tube spacing of the large-diameter SiCNT bundles was larger than that of the CNT bundles. The electronic structure calculations show that the inter-tube coupling leads to the splitting of the doubly degenerated states, reduction of the band-gap and the expansions of valence and conduction bands. It was shown that the polygonization of the SiCNTs in the bundle leads to a further dispersion of the occupied bands. Another notable effect of polygonization is an increase in the band-gap by 0.18 eV.

7. Nanotube–nanowire transformations

In addition to the use of nanowires as templates (or molds) in the fabrication of nanotubes, and vice versa, in various synthetic strategies, as described above and reviewed elsewhere [109], nanotube-to-nanowire, as well as nanowire-to-nanotube, transformations can also occur. We shall describe one example here.

7.1. From SiNW ⊂ AuNT to AuNW ⊂ SiO_2NT: SiNWs as sacrificial templates

The potential application of SiNWs in interconnection and as basic components in future mesoscopic electronic and optoelectronic devices raise the issues of electrical conductivity of SiNWs and the patterning of electrical (ohmic) contacts to SiNWs. A simple and effective technique to fabricate a metal thin film on the surface of SiNWs, or SiNWs wrapped with Au cable, was reported [110]. This particular nanostructure (Fig. 25) can be considered as a silicon nanowire encased within a gold nanotube (SiNW ⊂ AuNT).

When the heterostructure SiNW ⊂ AuNTs were furnace annealed at ~880 °C and 10^{-2} Torr, uniform crystalline AuNWs were formed in the core of the nanowire, with the SiNWs being oxidized to SiO_2 concomitantly [111]. Fig. 26 shows TEM images of an AuNW inside a SiO_x sheath. The resulting heterostructure may be designated as AuNW ⊂ SiO_2NT. This, in effect, is a "nanotube-to-nanowire" transformation for Au, and vice versa for Si. This transformation is a result of the softening of SiNWs upon oxidation and the enhanced Au diffusion at elevated temperatures, in combination with the inertness (resistance to oxidation) of the noble metal gold. The SiO_2 overlayer on AuNWs can be readily removed by HF etching to expose the AuNWs. Thus, this simple method can be used to synthesize very fine crystalline Au nanowires.

8. Photoluminescence and band-gap opening in quantum-size regime

Photoluminescence (PL) is the emission of light when a pair of electron and hole, created by absorption of a photon, recombine in a material. The wavelength of the luminescence is longer than that of the light being absorbed since part of the energy is lost to other nonradiative processes.

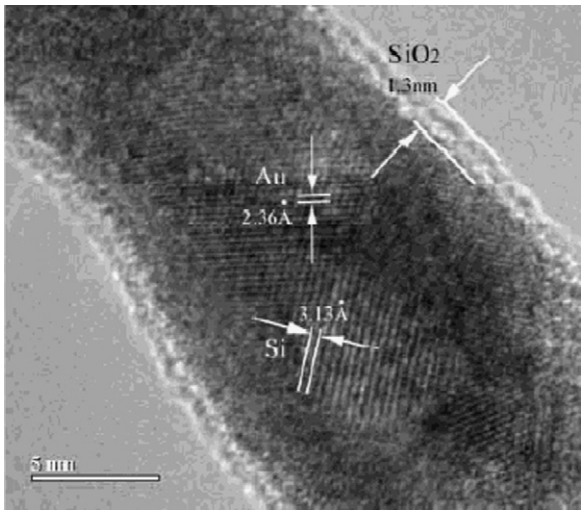

Fig. 25. A HRTEM image shows an Au film covering the SiNW, which is in turn covered by a SiO_2 layer of about 1 nm. (Reprinted with permission from Ref. [110]. Copyright 2002 American Chemical Society.)

It is well known that bulk silicon is an "indirect band-gap" semiconductor. When silicon is irradiated with a visible light, it emits radiation only weakly in the infrared region. This is because the radiative recombination of the electron–hole pair is very slow for an "indirect band-gap" semiconductor as the momentum is not conserved in the recombination process. Hence bulk silicon has traditionally been considered not a good photonic material.

As the size of a silicon nanomaterial is reduced, however, the situation changes. In the quantum-size regime (sizes on the order of 5 nm or less), silicon can gradually transform into a "direct band-gap" semiconductor. Here, two dramatic behaviorial changes occur: (1) it becomes a good light emitter; and (2) band-gap opening that changes the wavelength of the emitted light. We shall briefly describe each of these topics next.

8.1. Photoluminescence

When the size of a silicon nanomaterial is reduced to below 5 nm or less, it can gradually transform into a direct semiconductor. When silicon is illuminated with an ultraviolet light, the electron–hole pairs created are confined to a small dimension such that they attract each other strongly, thereby enhancing the radiative recombination process and thus photoluminescence efficiently. The "magic" dimension of 5 nm is the so-called Bohr radius of the exciton (the electron–hole pair) of silicon. In fact, silicon nanodots, silicon nanowires, and certain disordered forms of silicon exhibit efficient photoluminescence properties in this nanosize regime.

While the exact origin of these properties is still under investigation, it is generally believed that they arise from quantum-size effect. As will be described in the next subsection, the band-gap of SiNWs increases from the bulk value of 1.1 to 3.5 eV as the diameter of the nanowire decreases from 7 to 1.3 nm, respectively. Thus, the PL wavelength can be continuously tuned from the infrared, through the entire visible, to the ultraviolet spectra as the size is reduced from 5 to 1 nm, corresponding to the widening of the band-gap as the diameter of the nanowire is reduced successively. Similar trends were observed for SiNDs and porous silicon [112–115]. (Porous silicon is a sponge-like material that comprises an array of nanosized filaments containing SiNDs and SiNWs. For porous silicon, the particle size is inversely proportional to the extent of

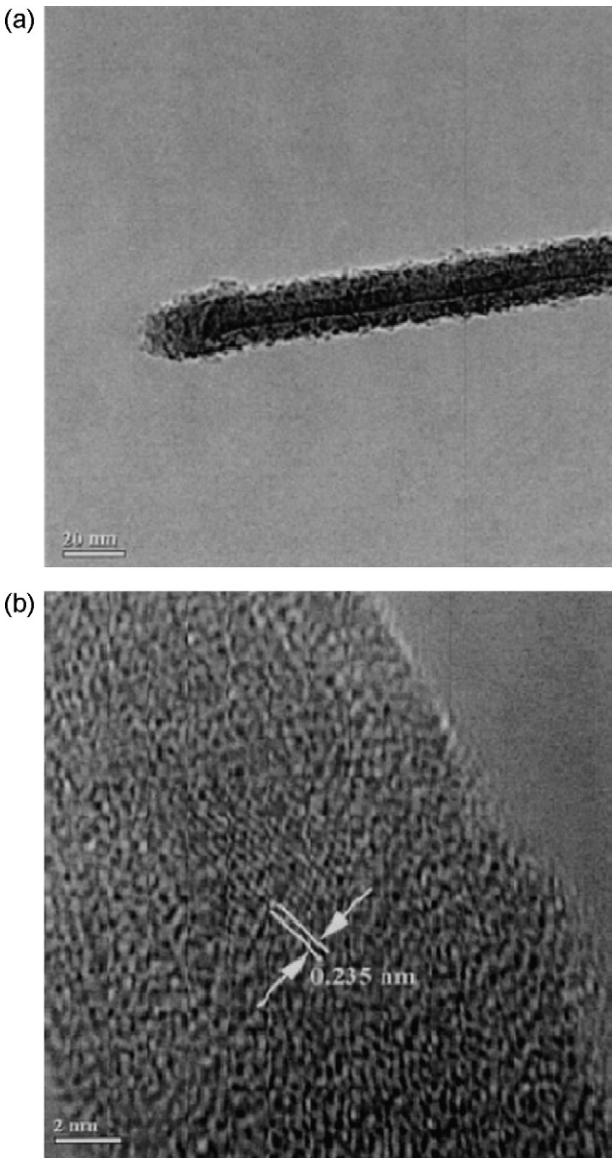

Fig. 26. (a) TEM image of AuNW inside a SiO_x sheath formed by annealing the Au-coated SiNW at 880 °C for 1 h at 10^{-2} Torr, and (b) the corresponding HRTEM image showing the Au core. (Reprinted with permission from Ref. [111]. Copyright 2004 American Institute of Physics.)

etching. Porous silicon can likewise be made to emit red, orange, yellow, green, and blue lights.)

Here we give one example of a strong photoluminescence from ultrafine silicon nanowires. Ultrafine SiNWs (1–5 nm in diameter), prepared with zeolites as templates, can exhibit very intense (orders of magnitude higher) luminescence in the PL measurement (Fig. 27, curve b) [55]. The PL peak centers around 720 nm. In contrast, very weak PL intensity was obtained from normal SiNW samples of 20–50 nm in diameter (Fig. 27, curve a). The PL peak centers at around 600 nm.

In recent years, silicon quantum dots and quantum wells and porous silicon have been used to fabricate LEDs and other optoelectronics (see reviews [116,117] and references cited therein).

8.2. Band-gap opening and indirect-to-direct band-gap transformation

Recently, Lee and coworkers reported band-gap opening of SiNWs due to quantum confinement effect when the diameter of SiNW shrinks to below 7 nm [118]. Scanning tunneling spectroscopy measurements were performed on individual oxide-removed SiNWs and were used to evaluate the electronic energy gaps as a function of nanowire diameter (Fig. 28). The energy gap increases with decreasing SiNW diameter, namely, from 1.1 eV for 7 nm to 3.5 eV for 1.3 nm in diameter, in agreement with the corresponding wavelength changes of the photoluminescence.

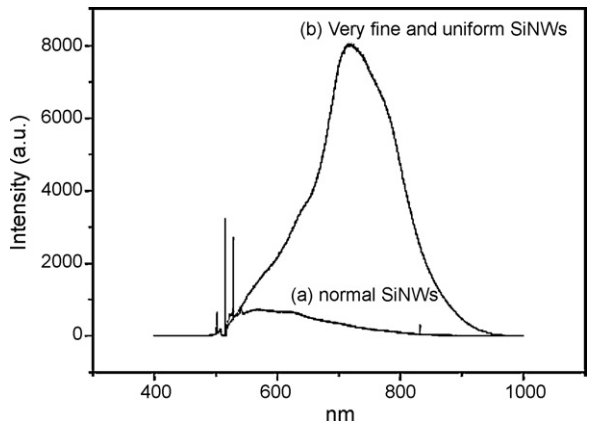

Fig. 27. Photoluminescence spectra from (a) normal SiNWs 20-50 nm in diameter and (b) very fine and uniform SiNWs 1–5 nm in diameter synthesized with zeolite Y. (Reprinted with permission from Ref. [55]. Copyright 2003 American Chemical Society.)

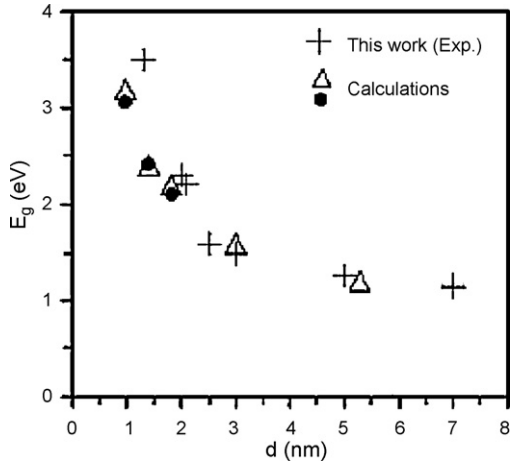

Fig. 28. Experimental band-gap vs. diameter for SiNWs. Also shown are the calculated diameter-dependent band-gaps (filled circles and triangles). (From Ref. [118] (http://www.sciencemag.org). Reprinted with permission from AAAS.)

The transition from an indirect band-gap to a direct band-gap of hydrogen- passivated SiNWs of diameters up to 4.2 nm along the <1 1 0> and <1 1 1> directions has been investigated theoretically by Zhao et al. [119]. These authors showed, via DFT calculations, that all <1 1 0> SiNWs in this size range exhibit a "direct" band-gap at Γ due to band folding, whereas the <1 1 1> SiNWs exhibit a transition from an indirect gap in large wires to a direct one in small wires. The gap increases subquadratically as the diameter decreases. The <1 1 1> wires have overall a slightly larger band-gap than <1 1 0> wires, as expected from the effective-mass difference.

9. Acronyms

In this section, we shall first give the acronyms of various commonly-used calculation methods, briefly state their applicabilities, accuracies, and limitations [120], followed by other common acronyms used in this review.

9.1. Acronyms of various calculation methods, their applications and limitations

AM1, CNDO, MNDO, PM3, ZDO All are semi-empirical methods, with AM1, MNDO, and PM3 based on the Neglect of Differential Diatomic Overlap (NDDO) integral approximation, while the older (and now-obsolete) CNDO uses an even simpler scheme. In fact, the aforementioned three models are Zero Differential Overlap (ZDO) methods, where two-electron integrals involving two-center charge distributions are neglected. Different parameterization schemes give rise to these methods. Among these three methods, AM1 and PM3 are more popular and yield comparable results. In a way, these semi-empirical methods are quick ways to yield the geometry and energy (in terms of heat of formation) for a relatively large system.

BPW91 Becke's exchange with the Perdew-Wang 1991 correlation functional, one of the more popular functionals used in DFT calculations.

B3LYP One commonly-used DFT functional is BLYP (Becke for treating the exchange portion and Lee, Yang, and Parr for the correlation part). To improve upon BLYP, we now have the hybrid functional B3LYP, where three parameters are used to specify how much of the Becke's exact exchange functional is mixed in. B3LYP is now one of the most popular hybrid functionals used in DFT calculations.

cc-pVTZ Correlation-consistent (cc) basis set, which includes a set of polarization (p) functions and whose valence (V) orbitals are of triple-zeta (TZ) quality. This is a fairly large basis set.

CCSD(T) An ab initio method in which the electronic correlation is treated by the coupled-cluster (CC) approach that takes into account all single (S) and double (D) excitations, while the triple (T) excitations are estimated perturbationally. This high-level method demands a lot of computational resources and, hence, is only applicable to fairly small systems.

CISD Configuration interaction method which includes all single and double excitations.

DFT Density-Functional Theory first determines the probability density ρ and then calculates the energy E of the system in terms of ρ. In other words, in DFT, E is a functional of ρ, which itself is a function of electronic coordinates. This method is gaining popularity rapidly because even its most elementary calculation includes correlation effect to a certain extent but takes roughly the same amount of time as a HF calculation, which completely neglects correlation.

DFTB, DFTB+ Density-Functional Tight-Binding Theory. The "+" sign signifies that van der Waals (and π interactions) are included via a Lennard-Jones dispersion correction scheme. DFTB+ is the latest version of Density-Functional Tight-Binding (DFTB) method developed by a group at Bremen University.

DFTB-MD Density-Functional Tight-Binding Molecular Dynamics (DFTB-MD) is a MD method that employs a tight-binding potential that, in terms of sophistication, lies somewhere between ab initio (or DFT) and empirical potentials. TB is better than the empirical potential methods because it explicitly takes into account the electronic structure of the system in a semi-empirical manner and it is several orders of magnitude faster than the DFT-based approach.

FP-LMTO-MD Full-potential linear-muffin-tin-orbital molecular dynamics method.

GTBMD Generalized Tight-Binding Molecular Dynamics (GTBMD) formulated by Menon and Subbaswamy allows for full relaxation of covalent systems with no symmetry constraints. This method yields results in good agreement with experimental and local density approximation (LDA) results for the structural and vibrational properties of fullerenes and nanotubes.

GGA Generalized Gradient Approximation (GAA) is one of the versions of DFT primarily used in physics.

GGA-PBE Perdew-Burke-Ernzerhof parametrization of the generalized gradient approximation.

Gaussian mn This is probably the most widely used and user-friendly software package around for quantum chemical calculations. It was first released in 1970 as Gaussian 70 and the latest version is Gaussian 09, issued in 2009. It does essentially every type of ab initio, DFT, and semi-empirical method. Its popularity is well earned.

HF The ab initio Hartree-Fock (HF) method assumes each electron (in a molecule) moves in an average potential generated by the nuclei and the remaining electrons. This assumption is flawed in that it ignores electron–electron correlation (see DFT). Such a calculation does not demand extensive computing resources. Hence it is applicable to fairly large systems.

HMO The Hückel Molecular Orbital (HMO) theory is likely the oldest and crudest semi-empirical method around. Besides being of historical interest, it is now only applied to exceedingly large systems that cannot be treated by any other methods.

LDA, LSDA Local Density Approximation (LDA) is an approximation to the exchange-correlation energy functional for unspin-polarized systems in DFT that depend solely on the value of electron density at each point in space. For spin-polarized systems, Local Spin Density Approximation (LSDA) is used.

MC The Monte Carlo (MC) method is a statistical simulation procedure in which random numbers are generated to examine the problem at hand. For example, solving problems involving a few atoms accurately is now possible, but the job for a large number (hundreds or even thousands) of atoms is much more daunting. With the MC methods, a large system is viewed as a number of random configurations, and that results obtained can be used to describe the system as a whole.

MD Molecular Dynamic (MD) is another form of computer simulation in which atoms and molecules are allowed to interact for a period of time, with the interaction being governed by potential functions approximating the dynamics of molecular systems. If the potential functions are inadequate, we will need to resort to the much more expensive ab initio MD method (see also DFTB-MD).

MP2 Møller and Plesset (MP) applied the perturbation theory to treat the electron correlation problem in 1930s. Even though this method has been around for a long time, the second-order (MP2) energy correction was not routinely calculated until the 1980s. Now even the fourth-order (MP4) or higher corrections have become very common. Since this approach is perturbational, it can give rise to energies that are lower than the exact values. Also, the trends of MP2-, MP3-, MP4-, ... corrected energies for many systems indicate that convergence may be slow, or even oscillatory.

PM3 Parameter model 3 (see AM1).

PW91 Perdew-Wang exchange-correlation functional used in DFT calculations.

QCISD(T), QCISD(FC) Quadratic Configuration Interaction (QCI), developed in the 1980s by Pople and coworkers, is a non-variational approach that is intermediate between CC (coupled-cluster) and CI (configuration interaction) methods. Similar to the CC methods, QCI also has the corresponding QCISD and QCISD(T) options. Both the CCSD(T) and QCISD(T) have been rated as the most reliable among the currently computationally affordable methods. A less expensive variant of QCISD(T) is QCISD(FC), where FC denotes the "frozen core" approximation. In this approximation, only the correlation energy associated with the valence electrons is calculated.

RHF Restricted Hartree-Fock (RHF) formalism applicable to calculations of closed-shell systems.

SP-DFT Spin-Polarized Density-Functional Theory.

TDDFT Time-Dependent Density-Functional Theory.

Composite methods In a composite method, instead of directly doing an expensive calculation such as CCSD(T) or QCISD(T) with a very large basis set, a series of less time-consuming "single-points" are carried out and an approximate energy is obtained by applying additive rules, considering various correction terms, etc. Currently, popular composite methods include Gaussian-n (Gn), Complete Basis Set (CBS), and Weizmann-n (Wn).

Gn There have been a series of Gaussian-n (Gn) methods: G1 in 1989, G2 in 1990, G3 in 1998, and G4 in 2007, all developed by Pople (1925-2004) and his coworkers. In addition, a number of variants of the G2 to G4 methods have also been proposed. Since G1 did not last very long, only G2, G3, and G4 will be discussed here. The G2 and G3 methods are approximations for the levels of theory of QCISD(T)/6-311 + G(3df,2p) and QCISD(T)/G3Large, where 6-311 + G(3df,2p) and G3Large are very large basis sets that make the calculations expensive. To test the accuracy of these methods, Pople and coworkers suggested a set of 148 very accurate gas-phase experimental data. For this set of data, the average absolute errors for G2 and G3 are 6.7 and 3.8 kJ/mol, respectively. Furthermore, it is noted that G3 is actually less expensive than G2, which shows the importance of designing a basis set judiciously. Experience indicates that, for systems of up to 10 non-hydrogen atoms, the expected absolute uncertainty for G2/G3 increases to about 10–15 kJ/mol. On the other hand, the G4 method yields a smaller mean absolute deviation (3.5 kJ/mol) from experiments, when compared with the G3 method (4.7 kJ/mol) on a test set of 454 energies. The G4 theory shows large improvement for ΔH_f in many types of molecules, including non-hydrogens, hydrocarbons, substituted hydrocarbons, inorganic hydrides, radicals, etc.

CBS The Complete Basis Set (CBS) is one of the more popular composite methods. Its variants include CBS-Q, CBS-q, and CBS-4. In these methods, special procedures are designed to estimate the complete basis set limit energy by extrapolation. Similar to the Gn methods, "single-point" calculations are also required in the CBS methods. For the aforementioned G2 test set of accurate data, the absolute errors for the CBS-Q, CBS-q and CBS-4 models are 6.7, 8.8, and 13.0 kJ/mol, respectively.

Wn Another series of composite computational methods, Weizmann-n (Wn), with $n = 1–4$, have been proposed by Martin and coworkers: W1 and W2 in 1999 and W3 and W4 in 2004. These models aim at approximating the CBS limit at the CCSD(T) level of theory. In the Wn methods, the core-valence correlation is done at the more advanced CCSD(T) level with a "specially designed" core-valence basis set. In comparison, in the G2 and G3 methods, the corresponding correlation is either ignored (G2) or calculated at a less sophisticated (MP2) level (G3).

9.2. Other acronyms

Other acronyms used in this review include:

1D one-dimensional
AAO anodized aluminum oxide
CBM conduction band minimum
CNTs carbon nanotubes
CNW carbon nanowire
cSiNTs crystalline silicon nanotubes
CVD chemical vapor deposition
DWSiNTs double-walled silicon nanotubes
DWSiCNTs double-walled silicon carbide nanotubes
EDS energy dispersive spectroscopy
EELS electron energy loss spectroscopy
HOMO highest occupied molecular orbital
HOVB highest occupied valence band
HRTEM high-resolution transmission electron microscopy
LDOS local density of states
LUCB lowest unoccupied conduction band
LUMO lowest unoccupied molecular orbital
NT nanotube
NW nanowire
pc polycrystalline
PDOS partial density of states
SiCNTs silicon carbide nanotubes
SiCNWs silicon carbide nanowires
SiH silicon monohydride
SiNTs silicon nanotubes
SiNWs silicon nanowires
SWCNTs single-walled carbon nanotubes
SWSiCNTs single-walled silicon carbide nanotubes
SWSiNTs single-walled silicon nanotubes
TEM transmission electron microscope
TM transition metal
VBM valence band maximum
VLS vapor–liquid–solid

10. Conclusions

In conclusion, the advent of nanotechnology allows man to change the fundamental properties of matter, tailor make materials with desirable attributes, and fabricate functional devices of any dimension. This is a true revolution in the history of science and technology.

Silicon-based nanotechnology is highly promising since it is compatible with conventional silicon microtechnology. To build a nanodevice, one needs to control and manipulate the properties, size and shape of materials at the nanometer level. While great progress has been made in recent years, many unanswered questions still remain. For example, the structure of a *bona fide* SiNT remains an open question, which clearly requires synergistic efforts between theoreticians and experimentalists. This review deals with the theoretical investigations of the atomic and electronic structures as well as the mechanical, optical, electrical, and magnetic properties of silicon-based nanomaterials, with special emphasis on nanotubes and nanowires. The generalities vs. particularities and the commonalities vs. peculiarities of various nanostructures of these nanomaterials are discussed, along with many critical theoretical issues of importance in the future experimental developments of these functional nanomaterials.

References

[1] S. Iijima, Nature 354 (1991) 56.
[2] J.W.G. Wildoer, L.C. Venema, A.G. Rinzler, R.E. Smalley, C. Dekker, Nature 391 (1998) 59.
[3] T.W. Odom, J.L. Huang, P. Kim, C.M. Lieber, Nature 391 (1998) 62.
[4] J.C. Charlier, P. Lambin, Phys. Rev. B 57 (1998) R15037.
[5] G. Zhou, W.H. Duan, B.L. Gu, Chem. Phys. Lett. 333 (2001) 344.
[6] N. Hamada, S. Sawada, A. Oshiyama, Phys. Rev. Lett. 68 (1992) 1579.
[7] R. Saito, G. Dresselhaus, M.S. Dresselhaus, Physical Properties of Carbon Nanotubes, Imperial College Press, London, 1998.
[8] M. Ouyang, J.L. Huang, C.L. Cheung, C.M. Lieber, Science 292 (2001) 702.
[9] P.C. Collins, M.S. Arnold, P. Avouris, Science 292 (2001) 706.
[10] S. Iijima, C. Brabec, A. Maiti, J. Bernholc, J. Chem. Phys. 104 (1996) 2089.
[11] A. Thess, R. Lee, P. Nikolaev, H.J. Dai, P. Petit, J. Robert, C.H. Xu, Y.H. Lee, S.G. Kim, A.G. Rinzler, D.T. Colbert, G.E. Scuseria, D. Tomanek, J.E. Fischer, R.E. Smalley, Science 273 (1996) 483.
[12] C. Journet, W.K. Maser, P. Bernier, A. Loiseau, M.L. DelaChapelle, S. Lefrant, P. Deniard, R. Lee, J.E. Fischer, Nature 388 (1997) 756.
[13] J.W. Mintmire, B.I. Dunlap, C.T. White, Phys. Rev. Lett. 68 (1992) 631.
[14] R. Saito, M. Fujita, G. Dresselhaus, M.S. Dresselhaus, Appl. Phys. Lett. 60 (1992) 2204.
[15] R. Saito, M.G. Dresselhaus, M.S. Dresselhaus, Phys. Rev. B 61 (2000) 2981.
[16] R. Saito, M. Fujita, G. Dresselhaus, M.S. Dresselhaus, Phys. Rev. B 46 (1992) 1804.
[17] A.M. Morales, C.M. Lieber, Science 279 (1998) 208.
[18] Y.F. Zhang, Y.H. Tang, N. Wang, D.P. Yu, C.S. Lee, I. Bello, S.T. Lee, Appl. Phys. Lett. 72 (1998) 1835.
[19] M. Zhao, Y. Xia, F. Li, R.Q. Zhang, S.T. Lee, Phys. Rev. B 71 (2005) 085312.
[20] G. Mpourmpakis, G.E. Froudakis, G.P. Lithoxoos, J. Samios, Nano Lett. 6 (2006) 1581.
[21] X.H. Sun, C.P. Li, W.K. Wong, N.B. Wong, C.S. Lee, S.T. Lee, B.K. Teo, J. Am. Chem. Soc. 124 (2002) 14464.
[22] R.Q. Zhang, Y. Lifshitz, S.T. Lee, Adv. Mater. 15 (2003) 636.
[23] R.Q. Zhang, Y. Lifshitz, D.D.D. Ma, Y.L. Zhao, Th. Frauenheim, S.T. Lee, S.Y. Tong, J. Chem. Phys. 123 (2005) 144703.
[24] A.J. Lu, R.Q. Zhang, S.T. Lee, Appl. Phys. Lett. 92 (2008) 203109.
[25] A.J. Lu, R.Q. Zhang, S.T. Lee, Appl. Phys. Lett. 91 (2007) 263107.
[26] K.H. Hong, J. Kim, S.H. Lee, J.K. Shin, Nano Lett. 8 (2008) 1335.
[27] X.B. Yang, R.Q. Zhang, Appl. Phys. Lett. 93 (2008) 173108.
[28] A.J. Lu, R.Q. Zhang, S.T. Lee, Nanotechnology 19 (2008) 35708.
[29] B. Aradi, L.E. Ramos, P. Deák, Th. Köhler, F. Bechstedt, R.Q. Zhang, Th. Frauenheim, Phys. Rev. B 76 (2007) 035305.
[30] T. Vo, A.J. Williamson, G. Galli, Phys. Rev. B 74 (2006) 045116.
[31] R. Rurali, N. Lorente, Phys. Rev. Lett. 94 (2005) 026805.
[32] R. Rurali, A. Poissier, N. Lorente, Phys. Rev. B 74 (2006) 165324.
[33] X.B. Yang, R.Q. Zhang, Appl. Phys. Lett. 94 (2009) 113101.
[34] M.V. Fernández-Serra, Ch. Adessi, X. Blase, Phys. Rev. Lett. 96 (2006) 166805.
[35] P.W. Leu, B. Shan, K. Cho, Phys. Rev. B 73 (2006) 195320.
[36] M.F. Ng, L.P. Zhou, S.W. Yang, L.Y. Sim, V.B.C. Tan, P. Wu, Phys. Rev. B 76 (2007) 155435.
[37] E. Durgun, N. Akman, C. Ataca, S. Ciraci1, Phys. Rev. B 76 (2007) 245323.
[38] E. Durgun, N. Akman, S. Ciraci, Phys. Rev. B 78 (2008) 195116.
[39] G. Giorgi, X. Cartoixà, A. Sgamellotti, R. Rurali, Phys. Rev. B 78 (2008) 115327.
[40] Y. Kim, H.J. Joyce, Q. Gao, H.H. Tan, C. Jagadish, M. Paladugu, J. Zou, A.A. Suvorova, Nano Lett. 6 (2006) 599.
[41] Y. Wang, V. Schmidt, S. Senz, U. Gösele, Nat. Nanotechnol. 1 (2006) 186.
[42] Z.G. Wu, J.B. Neaton, J.C. Grossman, Phys. Rev. Lett. 100 (2008) 246804.
[43] J.X. Cao, X.G. Gong, J.X. Zhong, R.Q. Wu, Phys. Rev. Lett. 97 (2006) 136105.
[44] J.X. Cao, X.G. Gong, R.Q. Wu, Phys. Rev. B 75 (2007) 233302.
[45] R.R. He, P.D. Yang, Nat. Nanotechnol. 1 (2006) 42.
[46] S.B. Fagan, R.J. Baierle, R. Mota Antonio, J.R. da Silva, A. Fazzio, Phys. Rev. B 61 (2000) 9994.
[47] R.Q. Zhang, H.-L. Lee, W.-K. Li, B.K. Teo, J. Phys. Chem. B 109 (2005) 8605.
[48] S.B. Fagan, R. Mota, R.J. Baierle, G. Paiva, A.J.R. da Silva, A. Fazzio, J. Mol. Struct. (THEOCHEM) 539 (2001) 101.
[49] A.S. Barnard, S.P. Russo, J. Phys. Chem. B 107 (2003) 7577.
[50] R.Q. Zhang, S.T. Lee, C.-K. Law, W.-K. Li, B.K. Teo, Chem. Phys. Lett. 364 (2002) 251.
[51] J. Sha, J.J. Niu, X.Y. Ma, J. Xu, X.B. Zhang, Q. Yang, D. Yang, Adv. Mater. 14 (2002) 1219.
[52] S.Y. Jeong, J.Y. Kim, H.D. Yang, B.N. Yoon, S.H. Choi, H.K. Kang, C.W. Yang, Y.H. Lee, Adv. Mater. 15 (2003) 1172.
[53] C. Mu, Y.X. Yu, W. Liao, X.S. Zhao, D.S. Xu, X.H. Chen, D.P. Yu, Appl. Phys. Lett. 87 (2005) 113104.
[54] J.Q. Hu, Y. Bando, Z.W. Liu, J.H. Zhan, D. Golberg, T. Sekiguchi, Angew. Chem. Int. Ed. 43 (2004) 63.
[55] B.K. Teo, C.P. Li, X.H. Sun, N.B. Wong, S.T. Lee, Inorg. Chem. 42 (2003) 6723.
[56] M.D. Crescenzi, P. Castrucci, M. Scarselli, M. Diociaiuti, P.S. Chaudhari, C. Balasubramanian, T.M. Bhave, S.V. Bhoraskar, Appl. Phys. Lett. 86 (2005) 231901.
[57] D.F. Perepichka, F. Rosei, Small 2 (2006) 22.
[58] G. Seifert, Th. Köhler, H.M. Urbassek, E. Hernández, Th. Frauenheim, Phys. Rev. B 63 (2001) 193409.
[59] J.W. Kang, J.J. Seo, H.J. Hwang, J. Nanosci. Nanotechnol. 2 (2002) 687.
[60] H.Y. Peng, N. Wang, Y.F. Zheng, Y. Lifshitz, J. Kulik, R.Q. Zhang, C.S. Lee, S.T. Lee, Appl. Phys. Lett. 77 (2000) 2831.
[61] L.C. Qin, X.L. Zhao, K. Hirahara, Y. Miyamoto, Y. Ando, S. Iijima, Nature 408 (2000) 50.
[62] N. Wang, Z.K. Tang, G.D. Li, J.S. Chen, Nature 408 (2000) 50.
[63] J.J.P. Stewart, J. Comput. Chem. 10 (1989) 209.
[64] M.J.S. Dewar, W. Thiel, J. Am. Chem. Soc. 99 (1977) 4899.
[65] M.W. Zhao, R.Q. Zhang, Y.Y. Xia, C. Song, S.T. Lee, J. Phys. Chem. C 111 (2007) 1234.
[66] A.K. Singh, V. Kumar, T.M. Briere, Y. Kawazoe, Nano Lett. 2 (2002) 1243.
[67] K.H. Janzon, H. Schafer, A.Z. Weiss, Anorg. Allg. Chem. 372 (1970) 87.
[68] A.K. Singh, T.M. Briere, V. Kumar, Y. Kawazoe1, Phys. Rev. Lett. 91 (2003) 146802.
[69] T. Dumitrica, M. Hua, B.I. Yakobson, Phys. Rev. B 70 (2004) 241303.
[70] E. Durgun, S. Tongay, S. Ciraci, Phys. Rev. B 72 (2005) 75420.
[71] T. He, M.W. Zhao, W.F. Li, X.H. Lin, X.J. Zhang, X.D. Liu, Y.Y. Xia, L.M. Mei, Nanotechnology 19 (2008) 205707.
[72] M.W. Zhao, R.Q. Zhang, Y.Y. Xia, J. Appl. Phys. 102 (2007) 024313.
[73] A. Palaria, G. Klimeck, A. Strachan, Phys. Rev. B 78 (2008) 205315.
[74] C.P. Li, X.H. Sun, N.B. Wong, C.S. Lee, S.T. Lee, B.K. Teo, Chem. Phys. Lett. 365 (2002) 22.
[75] B.H. Yan, G. Zhou, J. Wu, W.H. Duan, B.L. Gu, Phys. Rev. B 73 (2006) 155432.
[76] B.H. Yan, G. Zhou, X.C. Zeng, J. Wu, B.L. Gu, W.H. Duan, Appl. Phys. Lett. 91 (2007) 103107.
[77] G.L. Harris, Properties of Silicon Carbide, INSPEC, Institution of Electrical Engineers, London, 1995.
[78] P. Mélinon, B. Masenelli, F. Tournus, A. Perez, Nat. Mater. 6 (2007) 479.
[79] H.W. Shim, H.C. Huang, Appl. Phys. Lett. 90 (2007) 083106.
[80] S.C. Chiu, Y.Y. Li, J. Cryst. Growth 311 (2009) 1036.
[81] Z.H. Wang, M.W. Zhao, T. He, X.J. Zhang, Z.X. Xi, S.S. Yan, X.D. Liu, Y.Y. Xia, J. Phys. Chem. C 113 (2009) 856.
[82] H.W. Shim, Y.F. Zhang, H.C. Huang, J. Appl. Phys. 104 (2008) 063511.
[83] N. Papanikolaou, J. Phys.: Condens. Mater. 20 (2008) 135201.
[84] B.H. Yan, G. Zhou, W.H. Duan, J. Wu, B.L. Gu, Appl. Phys. Lett. 89 (2006) 023104.
[85] M.A. Makeev, D. Srivastava, M. Menon, Phys. Rev. B 74 (2006) 165303.
[86] Z.G. Wang, X.T. Zu, F. Gao, W.J. Weber, Phys. Rev. B 77 (2008) 224113.
[87] T.Y. Zhang, M. Luo, W.K. Chan, J. Appl. Phys. 103 (2008) 104308.
[88] Z.W. Pan, H.L. Lai, F.C.K. Au, X.F. Duan, W.Y. Zhou, W.S. Shi, N. Wang, C.S. Lee, N.B. Wong, S.T. Lee, S.S. Xie, Adv. Mater. 12 (2000) 1186.
[89] Z.L. Wang, Z.R. Dai, R.P. Gao, Z.G. Bai, J.L. Gole, Appl. Phys. Lett. 77 (2000) 3349.
[90] Y. Zhang, T. Ichihashi, E. Landree, F. Nihey, S. Iijima, Science 285 (1999) 1719.
[91] L. Moro, A. Paul, D.C. Lorents, R. Malhotra, R.S. Ruoff, P. Lazzeri, L. Vanzetti, A. Lui, S. Subramoney, J. Appl. Phys. 81 (1997) 6141.
[92] A. Mavrandonakis, G.E. Froudakis, Nano Lett. 3 (2003) 1481.
[93] M. Menon, E. Richter, A. Mavrandonakis, G. Froudakis, A.N. Andriotis, Phys. Rev. B 69 (2004) 115322.
[94] Y.F. Zhang, H.C. Huang, Comput. Mater. Sci. 43 (2008) 664.
[95] S.-P. Huang, D.-S. Wu, J.-M. Hu, H. Zhang, Z. Xie, H. Hu, W.-D. Cheng, Opt. Express 15 (2007) 10947.
[96] B. Baumeier, P. Krüger, J. Pollmann, Phys. Rev. B 76 (2007) 085407.
[97] V.A. Margulis, E.A. Gaiduk, E.E. Muryumin, O.V. Boyarkina, L.V. Fomina, Phys. Rev. B 74 (2006) 245419.
[98] G. Alfieri, T. Kimoto, Phys. Status Solidi B 246 (2009) 407.
[99] S.-P. Huang, W.-D. Cheng, J.-M. Hu, Z. Xie, H. Hu, H. Zhang, J. Chem. Phys. 129 (2008) 174108.
[100] K.M. Alam, A.K. Ray, J. Comput. Theory Nanosci. 6 (2009) 16.
[101] M.W. Zhao, Y.Y. Xia, R.Q. Zhang, S.T. Lee, J. Chem. Phys. 122 (2005) 214707.
[102] F. Li, Y.Y. Xia, M.W. Zhao, X.D. Liu, B.D. Huang, Z.H. Yang, Y.J. Ji, C. Song, J. Appl. Phys. 97 (2005) 104311.
[103] T. He, M.W. Zhao, Y.Y. Xia, W.F. Li, C. Song, X.H. Lin, X.D. Liu, L.M. Mei, J. Chem. Phys. 125 (2006) 194710.
[104] J.X. Zhao, Y.H. Ding, J. Phys. Chem. C 112 (2008) 2558.
[105] R.J. Baierle, P. Piquini, L.P. Neves, R.H. Miwa, Phys. Rev. B 74 (2006) 155425.
[106] A. Gali, Phys. Rev. B 73 (2006) 245415.
[107] R. Moradian, S. Behzad, R. Chegel, Physica B 403 (2008) 3623.
[108] R. Moradian, S. Behzad, R. Chegel, J. Phys.: Condens. Mater. 20 (2008) 465214.
[109] B.K. Teo, X.H. Sun, Chem. Rev. 107 (2007) 1454.
[110] C.P. Li, X.H. Sun, N.B. Wong, C.S. Lee, S.T. Lee, B.K. Teo, J. Phys. Chem. B 106 (2002) 6980.
[111] T.C. Wong, C.P. Li, R.Q. Zhang, S.T. Lee, Appl. Phys. Lett. 84 (2004) 407.
[112] A.G. Cullis, L.T. Canham, P.D.J. Calcott, J. Appl. Phys. 82 (1997) 909.
[113] D.J. Lockwood, Solid State Commun. 92 (1994) 101.
[114] K.H. Jung, S. Shih, D.L. Kwong, J. Electrochem. Soc. 140 (1993) 3046.
[115] L.T. Canham, T.I. Cox, A. Loni, A. Simons, J. Appl. Surf. Sci. 102 (1996) 436.
[116] R.A. Soref, Proc. IEEE 81 (1993) 1687.
[117] N. Koshida, N. Matsumoto, Mater. Sci. Eng. R 40 (2003) 169.
[118] D.D.D. Ma, C.S. Lee, F.C.K. Au, S.Y. Tong, S.T. Lee, Science 299 (2003) 1874.
[119] X. Zhao, C.M. Wei, L. Yang, M.Y. Chou, Phys. Rev. Lett. 92 (2004) 236805.
[120] W.-K. Li, G.-D. Zhou, T.C.W. Mak, Advanced Structural Inorganic Chemistry, Oxford University Press, Oxford, 2008.